fluids

MDPI

Article

Modeling of Soluble and Biodegradable Contaminant Transport in Channels and Rivers

Luis Américo Carrasco-Venegas [1,*], Juan Taumaturgo Medina-Collana [2], Luz Genara Castañeda-Pérez [3], Aurelio Carrasco-Venegas [4], Daril Giovanni Martínez-Hilario [2], José Vulfrano González-Fernández [5,*], César Gutiérrez-Cuba [2], Héctor Ricardo Cuba-Torre [2], Lia Elis Concepción-Gamarra [6], Rodolfo Paz-Salazar [2] and Salvador Apolinar Trujillo-Pérez [2]

1 Centro de Investigación en Bioenergía, Universidad Nacional del Callao, Callao 15001, Peru
2 Facultad de Ingeniería Química, Universidad Nacional del Callao, Callao 15001, Peru
3 Facultad de Ciencias Naturales y Matemática, Universidad Nacional Federico Villareal, Lima 15001, Peru
4 Facultad de Ciencias Biológicas, Universidad Nacional de San Cristóbal de Huamanga, Ayacucho 05001, Peru
5 Instituto Tecnológico de San Luis Potosí, Tecnológico Nacional de México, San Luis Potosí 78436, Mexico
6 Facultad de Ingeniería Geológica, Minera, Metalúrgica y Geográfica, Universidad Nacional Mayor de San Marcos, Lima 15001, Peru
* Correspondence: lacarrascov@unac.edu.pe (L.A.C.-V.); jose1.gf@slp.tecnm.mx (J.V.G.-F.)

Abstract

Accurate prediction of contaminant transport and self-purification processes in rivers remains challenging because pollutant dispersion, biochemical reactions, and hydrodynamic conditions interact across multiple spatial scales. This study aims to develop and compare mathematical models for soluble contaminant transport and biodegradable organic matter removal in channels and rivers. Unsteady advection–diffusion–reaction equations were formulated for one-dimensional (1D), two-dimensional (2D), and three-dimensional (3D) transport scenarios and solved through numerical techniques based on the transformation of partial differential equations into systems of ordinary differential or algebraic equations. In parallel, the classical Streeter–Phelps model and an extended formulation incorporating turbulent diffusion were implemented to evaluate organic load degradation and oxygen deficit dynamics. Simulations were performed using a Matlab R2019a-based computational framework under representative hydraulic and reaction conditions obtained from literature data and empirical correlations. The results showed that, under specific conditions, the 3D model reproduced trends comparable to those predicted by the 2D model, while the latter approached the behavior of the 1D formulation. The Streeter–Phelps model predicted an organic load removal efficiency of 97.74%, a purification index of 1.9564, a critical time of 18.43 h, and a critical distance of 6.93 km. These findings provide a useful framework for river water-quality assessment and support future applications involving complex hydrodynamic and pollutant-loading scenarios.

Keywords: contaminant transport; water quality modeling; Streeter–Phelps model; advection–diffusion–reaction equations; turbulent dispersion; method of lines; mathematical modeling

Check for updates

Academic Editor: Moran Wang

Received: 10 May 2026
Revised: 14 June 2026
Accepted: 17 June 2026
Published: 20 June 2026

Copyright: © 2026 by the authors. Licensee MDPI, Basel, Switzerland. This article is an open access article distributed under the terms and conditions of the Creative Commons Attribution (CC BY) license.

1. Introduction

Water pollution in channels and rivers is a significant global problem with adverse consequences, primarily attributed to anthropogenic activities and, to a lesser extent, natural processes. Industrial effluents originate from factories and industrial plants that

discharge contaminants such as heavy metals, chemicals, and untreated wastewater [1–5]; the use of pesticides and fertilizers in agricultural runoff transports harmful substances [2,6]; untreated sewage and wastewater contain pathogens and organic pollutants [2,7,8]; as well as mining and metallurgical activities [1,9].

All these problems generate risks to human health and ecosystems in general; contaminated water is one of the main causes of disease and death worldwide; more than 14,000 people die daily due to water-related diseases [8,10,11]; common health problems include diarrhea, cholera, and other waterborne diseases [2,8]; contaminants such as heavy metals and microplastics negatively affect aquatic ecosystems, causing the death of fish and other marine organisms [3,5]; the degradation of water quality increases the cost of water treatment and affects agricultural productivity, generating economic losses [7].

Studies conducted in Dhaka, Bangladesh show that the Buriganga River is severely contaminated due to industrial waste, transportation, and improper waste disposal, which seriously affects public health [12]. Rivers in India, such as those in the Tiruppur area, suffer from high levels of pollution, forcing residents to rely on bottled water for drinking [8]. On the other hand, in semi-arid regions of Brazil, water quality is compromised by agricultural practices, leading to high levels of salinity and heavy metals in water sources [13].

Among mitigation and management strategies, the implementation of stricter regulations on industrial discharges and good practices can help reduce pollution levels [5,6]; the use of green technologies, nanotechnologies, and bioremediation methods can effectively treat and purify contaminated water [3,14]; educating communities about the importance of water conservation and pollution prevention can promote better environmental practices [12,15].

The study of water pollution modeling in rivers and channels is crucial due to its multiple impacts on environmental, social, economic, technological, and health aspects, mainly because of the environmental impact that affects aquatic ecosystems, causing a reduction in biodiversity, habitat degradation, and the proliferation of toxic algae [16,17]; the presence of contaminants such as heavy metals, organic substances, and nutrients can alter the natural balance and cause long-term ecological damage [18,19]; it also affects water quality, since pollution from industrial, agricultural, and urban sources can lead to deterioration of water quality, affecting both surface and groundwater systems. Regarding social impact, contaminated water represents serious health risks for communities that depend on these sources for drinking, bathing, and irrigation; contaminants such as fecal bacteria, nitrates, and chemical substances can cause various health problems [16,18]; increasing public awareness about water pollution and its consequences is vital to promote conservation efforts and sustainable water management practices [20,21].

Regarding the economic impact, the implementation of water quality models can reduce costs associated with treating contaminated water by optimizing the required interventions [6,21,22]. Furthermore, effective water management contributes to sustainable economic development, particularly in urban and agricultural regions where water resources are critical for productive activities [23,24].

From a technological perspective, the use of advanced water quality models im-proves the accuracy and efficiency of water resource assessment and management [17,25]. In addition, simulation and forecasting tools support decision-making processes by enabling better planning and faster responses to pollution events, thereby improving risk management strategies [26,27].

Water quality modeling also has important implications for public health. Monitoring and controlling water pollution are essential for preventing waterborne diseases and ensuring safe water for human consumption. Reliable predictive models can help identify

pollution sources, evaluate potential risks, and support the implementation of timely mitigation measures.

The modeling of contaminant transport is based on mass transport equations that account for concentration variations, advective and diffusive transport, kinetic reactions, and possible point sources. The Generalized Integral Transform Technique provides numerical or analytical solutions for predicting the dispersion of dissolved contaminants in rivers, streams, and channels, allowing the use of non-uniform velocity profiles and turbulent diffusion coefficients [28]. Computational fluid dynamics (CFD) models simulate the dispersion of soluble substances using the finite volume method to solve momentum, mass, and species conservation equations, incorporating Cartesian coordinate systems and zero-order turbulence models [29,30]. The Streeter–Phelps model, the first water quality model, predicts the concentration of organic matter and dissolved oxygen along rivers and, together with CFD approaches, supports the assessment of multiple effluent discharges [29,30]. Several models have since been derived from their original formulation.

Three-dimensional hydrodynamic models are widely used to establish and validate diffusion models and to predict contaminant concentration variations in representative river sections [31,32]. Another commonly applied approach is the one-dimensional advection–dispersion equation, which predicts the spatial and temporal distribution of dissolved substances and incorporates longitudinal dispersion coefficients determined through salt dilution experiments [33].

The hybrid mixing model was developed to overcome limitations of mixing cell-based models and has been applied to simulate contaminants such as ammonia, considering transformation processes and algal uptake [34]. Likewise, dispersion models in surface flows employ techniques such as the Petrov–Galerkin method and the discrete phase model to describe the transport of particles and dissolved substances in turbulent conditions [35,36]. Each of these approaches offers specific advantages depending on the application.

Contaminant transport modeling describes the movement, dispersion, settling, and transformation of pollutants under hydrodynamic and biogeochemical conditions. It enables the simulation of contaminant dynamics under varying flow regimes, discharges, and extreme events, supports the development of discharge control policies and risk assessments, complements field monitoring through predictive analyses, and contributes to the design of treatment systems and river restoration projects.

Finally, the objective of this work is to develop and analyze one-dimensional, two-dimensional, and three-dimensional mathematical models to describe the transport and dispersion of soluble contaminants in rivers and channels based on mass conservation equations. This study addresses the limited comparative evaluation of multidimensional transport models and the need for integrated approaches capable of representing both contaminant dispersion and water quality dynamics under a common modeling framework. To this end, classical analytical techniques and computational numerical methods are applied to assess the accuracy, advantages, and limitations of each approach. The proposed models provide predictive tools for understanding the spatiotemporal behavior of contaminants, supporting water quality management, and establishing technical guidelines for mitigating environmental impacts in surface water bodies.

2. Materials and Methods

2.1. Transport Model Parameters

2.1.1. Flow Parameters

Velocity profile

In some cases, it is necessary to consider vertical and transverse velocity profiles to obtain an accurate representation of contaminant transport, depending on whether the flow velocity is laminar or turbulent [37,38].

The velocity profile for laminar flow is obtained from the Navier–Stokes equation in rectangular coordinates, considering that the flow direction is the x-direction and that it depends on the transverse coordinate y and the vertical coordinate z; which is simplified using the continuity equation.

Navier–Stokes equation:

$$\rho \frac{DV}{Dt} = -\nabla p + \mu \nabla^2 V + \rho g. \quad (1)$$

Considering the flow in the x-direction, the Navier–Stokes equation is expanded as:

$$\rho\left(\frac{\partial V_x}{\partial t} + V_x\frac{\partial V_x}{\partial x} + V_y\frac{\partial V_x}{\partial y} + V_z\frac{\partial V_x}{\partial z}\right) = -\frac{\partial p}{\partial x} + \mu\left(\frac{\partial^2 V_x}{\partial x^2} + \frac{\partial^2 V_x}{\partial y^2} + \frac{\partial^2 V_x}{\partial z^2}\right) + \rho g_x. \quad (2)$$

Continuity equation:

$$\frac{\partial \rho}{\partial t} = -\nabla.\rho V. \quad (3)$$

Considering an incompressible fluid (ρ) constant, the continuity equation becomes:

$$\frac{\partial V_x}{\partial x} + \frac{\partial V_y}{\partial y} + \frac{\partial V_z}{\partial z} = 0. \quad (4)$$

Since the fluid moves by advection only in the x-direction, the velocities in the other directions are zero, therefore from Equation (2): $\frac{\partial V_x}{\partial x} = 0$ and additionally, $\frac{\partial^2 V_x}{\partial x^2} = 0$. It is considered that natural flow in channels and rivers depends only on the gravitational field reflected in the slope; pressure differences do not intervene; consequently, Equation (2) becomes:

$$\mu\left(\frac{\partial^2 V_x}{\partial y^2} + \frac{\partial^2 V_x}{\partial z^2}\right) + \rho g_x = 0, \quad (5)$$

$$g_x = g sin(\theta)$$

V_x, V_y, V_z: Components of velocity vector V in rectangular coordinates (m s^{-1}).
ρ: Fluid density (kg m^{-3}).
x, y, z: Components of the rectangular coordinate system (m).
μ: Fluid viscosity (kg m^{-1} s^{-1}).
g: Gravitational field (m s^{-2}).
∇p: Pressure gradient (kg m^{-2} s^{-2}).
θ: Angle formed by the horizontal and the flow direction.

Equation (5) is the Poisson equation, whose solution using the Fourier transform [39,40] is given by:

$$V_x(y,z) = \frac{4\rho g sin(\theta) H^2}{\mu \pi^3} \sum_{1,3,5\ldots}^{\infty} \frac{1}{n^3}\left[1 - \frac{cosh(\frac{n\pi y}{H})}{cosh(\frac{n\pi W}{H})}\right] \times sin(\frac{n\pi z}{H}). \quad (6)$$

An empirical equation that provides values very close to the analytical solution has the form shown in Equation (7):

$$V_x(y,z) = V\left[1-\left(\frac{y}{W}\right)^2\right]\left[1-\left(\frac{z}{H}\right)^2\right], \quad (7)$$

$V_x(y,z)$: Local velocity in the x-direction (m s^{-1}).
V_{max}: Maximum velocity at the center of the channel (y = 0 and z = 0) (m s^{-1}).
W: Half-width of the channel (m); $y \in [-W,\ W]$.
H: Channel height (m); $z \in [0,\ H]$.

In modeling, it is simpler to use Equation (7) since it satisfies the following characteristics: no-slip conditions at the walls $V_x(y,z) = 0$ at $y = \pm W$, $z = 0$ and $z = H$; it is easy to use in contaminant transport models (it does not require infinite series); it adequately represents the flattening of the profile due to the lateral and upper/lower walls; V_{max} can be calibrated with experimental data or from flow rate measurements.

In very wide channels $W \to \infty$, this formula reduces to the classical parabola as a function of z:

$$V_x(z) = V\left[1-\left(\frac{z}{H}\right)^2\right]. \quad (8)$$

For the case of turbulent flow, an empirical velocity profile or a plug flow profile is considered.

Volumetric flow

The volumetric flow or water flow velocity is a fundamental parameter that affects the dispersion of contaminants. In non-uniform flows, the velocity may vary spatially, which complicates the solution of the advection–dispersion equations [37,41,42]; however, for a certain flow reach, the discharge is constant.

The discharge is obtained by integrating the velocity profile described by Equation (6), Equation (7), or Equation (8), as appropriate.

$$Q = \int_{-W}^{W}\int_{0}^{H} V_x(y,z)\,dz\,dy. \quad (9)$$

In conclusion, to apply contaminant transport equations, it is necessary to know the velocity distribution equation, the mean and/or maximum velocity, and the discharge in both laminar and turbulent regimes in water flows such as channels and rivers.

2.1.2. Turbulent Diffusion Coefficients

To obtain the longitudinal, transverse, and vertical dispersion coefficients in rivers and channels, various analytical, empirical, and statistical equations are used that consider the hydraulic and geometric characteristics of the flow; some of them are illustrated.

Longitudinal diffusion coefficient (D_L)

Statistical moments method: This method constructs two systems of moments, spatial and temporal, without the need to solve higher-order partial differential equations. This method is applied in any stationary velocity field that is periodic in the flow direction and heterogeneous in porosity [43,44].

The longitudinal dispersion coefficient is calculated from the derivative of the spatial variance with respect to time, that is:

$$D_X = \frac{1}{2}\frac{d\sigma^2_{(x)}}{dt}. \quad (10)$$

From an experimental point of view, it is much more feasible to obtain the temporal variance rather than the spatial variance, since determining spatial variance requires monitoring at several points at the same instant, which implies greater logistical effort such as measurement equipment and personnel, whereas temporal variance only requires measurement at two specific points downstream from the discharge point; the relationship between both types of variance is given by:

$$\sigma^2_{(x)} = U^2 \times \sigma^2_{(t)}. \tag{11}$$

The temporal variance, which is the measure of dispersion around the centroid of the concentration averaged across the cross section, is defined as:

$$\sigma^2_t = \frac{\int_{-\infty}^{\infty}(t-\bar{t})^2 C(x,t)dt}{\int_{-\infty}^{\infty} C(x,t)dt}. \tag{12}$$

where the centroid travel time t is given by:

$$\bar{t} = \frac{\int_{-\infty}^{\infty} t \times C(x,t)dt}{\int_{-\infty}^{\infty} C(x,t)dt}. \tag{13}$$

The denominator of Equations (12) and (13) is called the zero-order statistical moment. Equation (13) is called the first-order statistical moment, and Equation (12) is called the second-order statistical moment. Therefore, the dispersion coefficient is obtained explicitly as:

$$D_x = \frac{1}{2}U^2 \frac{\sigma^2_t(x_2) - \sigma^2_t(x_1)}{\overline{t_2} - \overline{t_1}}, \tag{14}$$

$\sigma^2_{(t)}$: Temporal variance of the tracer concentration across a cross section at the specified locations x_1 y x_2 along the course of a river or channel.

U: Mean velocity of displacement of the tracer cloud centroid (m s^{-1}).

To determine the longitudinal dispersion coefficient, it is necessary to transform the continuous Equations (12) and (13) into discrete equations that allow the use of concentration data obtained in the field through tracers.

The zero-order statistical moment is calculated as:

$$\mu_0 = \sum_1^n \left[\frac{C(t_i) + C(t_{i-1})}{2}\right] \times \Delta t_i. \tag{15}$$

The first-order statistical moment is obtained as:

$$\mu_1 = t_p = \frac{\sum_1^n t_i \left[\frac{C(t_i)+C(t_{i-1})}{2}\right]}{\mu_0} \times \Delta t_i. \tag{16}$$

The second-order statistical moment is obtained as:

$$\mu_2 = \sigma^2_t = \frac{\sum_1^n (t_i - t_p)^2 \left[\frac{C(t_i)+C(t_{i-1})}{2}\right]}{\mu_0} \times \Delta t_i. \tag{17}$$

The turbulent diffusion coefficient, also known as the *longitudinal dispersion coefficient*, varies over a wide range of reported values; according to Fischer [45] and subsequent works [46,47], the variation range is between 10^{-2} $m^2/s \leq D_L \leq 10^6$ m^2/s.

Transverse diffusion coefficient (D_T)

Several theoretical and empirical equations have been proposed to estimate transverse dispersion coefficients in channels and rivers, depending on the hydraulic and geometric characteristics of the flow. Among these, the formulation proposed by Elder is one of the most widely used and influential approaches for predicting transverse dispersion in open-channel flows [47,48]. Additional empirical formulations commonly reported in the literature are summarized in Appendix A.

Classical Elder formula [46]:

$$D_T = \alpha U^* H \tag{18}$$

α: Elder empirical constant (0.15).

Fischer et al. formula [49]. Uses an equation similar to Elder's:

$$D_T = 0.6 U^* H. \tag{19}$$

Typical values of these coefficients range as follows:

Laboratory channels: $D_T = 10^{-3} - 10^{-1}$ m^2 s^{-1}; medium rivers $D_T = 10^{0} - 10^{1}$ m^2 s^{-1}; large rivers: $D_T = 10^{1} - 10^{2}$ m^2 s^{-1}.

In conclusion, the equations and methods for calculating transverse dispersion coefficients vary depending on the specific flow conditions and available data. The selection of the appropriate method can be optimized using criteria based on aspect ratio, roughness, and channel sinuosity, as well as the availability of secondary current data [47,48,50].

It is important to incorporate in the analysis the Peclet number, defined as the ratio between advective and diffusive transport, that is $P_e = U\Delta x/D$; if Pe > 1 advective transport dominates; otherwise, diffusive transport dominates [50].

Vertical diffusion coefficient (D_V)

Normally, the contribution of this coefficient is small; however, it has influence especially in laminar flows that are governed by diffusion coefficients whose values are much smaller compared to those of turbulent flow [46,51].

Elder formula:

$$D_V = 0.067 \times U^* H \tag{20}$$

The formula presented is linear and has the same units as the longitudinal diffusion coefficient. To calculate vertical dispersion coefficients in channels and rivers, several equations and methods can be used, each with its own advantages and limitations. The choice of the appropriate method will depend on the specific characteristics of the channel or river, as well as the availability of hydraulic and geometric data [52].

Use of tracers

Common tracers used to measure dispersion coefficients in rivers and channels must be harmless to the aquatic environment; several types are used. Visible dyes such as Rhodamine WT are widely used due to their visibility and ease of detection. These dyes allow the measurement of dispersion through remote sensing and in situ detection techniques and have proven effective even under high turbidity conditions [53]; In some studies, salts are used as tracers due to their ease of detection through water conductivity, especially in studies of hydraulic connectivity in mines, where they have proven effective and safe [54]; Other tracers such as radioisotopes are also used [55], among many other techniques depending on resource availability.

Solubility of oxygen from air under various conditions

To develop the modeling of the degradation of organic substances, it is necessary to know the solubility of oxygen under various conditions of temperature, pressure, and salt content, which can be obtained using Henry's law or other empirical equations.

The solubility of oxygen in aqueous solutions of salts such as KCl, K_2SO_4 and $CaCl_2$ can be adjusted using a Setschenow-type equation. This equation considers temperature and the molality of the salts present in the solution [56]; For saline solutions at atmospheric pressure, a generalized expression is presented that includes Henry's constant to account for temperature effects and the Setschenow parameter for salt content [57]; however, these correlations do not include variation with partial pressure. For moderate concentrations, the equation proposed by Debelius is used [58].

According to Chapra and Ji [59,60], based on APHA (American Public Health Association), which is used by QUAL2K models, the oxygen concentration in water as a function of temperature at a pressure of 1 atm is calculated using the equation:

$$lnO_{Sf} = -139.3441 + \frac{1.575701 \times 10^5}{T_K} - \frac{6.642308 \times 10^7}{T_K^2} + \frac{1.2438 \times 10^{10}}{T_K^3} - \frac{8.621949 \times 10^{11}}{T_K^4}. \quad (21)$$

The solubility of oxygen in water with salt content is obtained using:

$$lnO_{SS} = LnO_{sf} - S(1.7674 \times 10^{-2} - \frac{1.0754 \times 10^1}{T_K} + \frac{2.1407 \times 10^3}{T_K^4}). \quad (22)$$

Temperature must be expressed in Kelvin, and salt concentration (S), in s g L^{-1}.

The empirical equation that determines oxygen solubility from air as a function of total pressure, given by the EPA [61], is:

$$O_{sp} = O_{sf} \times P \left[\frac{(1 - \frac{P_{wv}}{P})(1 - \theta \times P)}{(1 - P_{wv})(1 - \theta)} \right], \quad (23)$$

$$lnP_{wv} = 11.8571 - \frac{3840.70}{T_K} - \frac{216.961}{T_K^2}, \quad (24)$$

$$\theta = 0.0000975 - 1.426 \times 10^{-5} \times T + 6.436 \times 10^{-8} \times T^2, \quad (25)$$

P_{wv}: Water vapor pressure (mmHg).
P: Total pressure (mmHg).
T: Temperature (C).
T_K: Temperature (K).
O_{sf}, O_{ss}, O_{sp}: Oxygen solubility as a function of pressure (mg L^{-1}).

There are many other equations for calculating oxygen solubility under the described conditions; however, these three equations are sufficient to estimate solubility for a specific case as indicated by the EPA [61].

2.1.3. Kinetic Constants

Kinetic constants refer to the rate of "consumption" or "generation" of the chemical species being tracked; they include processes such as losses by adsorption in sediments, chemical transformations, and gas solubilization processes such as oxygen, which is important in the oxidation of biodegradable organic matter.

In water quality models, nitrification is usually represented by multiplying the base reaction rate by attenuation factors associated with water temperature and dissolved oxygen. However, in most cases, the effect of other important variables such as pH, substrate availability, and nitrifying bacteria dynamics is neglected. The ammonium oxidation constant is 2.03 day^{-1} at pH 7 and the nitrite-to-nitrate oxidation constant is 2.33 day^{-1} at pH 7 [62].

Regarding the presence of organic load in rivers or channels, water quality is modeled using the Streeter–Phelps equations and their modifications, which involve the use of the deoxygenation constant k_1 and the reaeration constant k_2.

It is also important to analyze the Damköhler number (Da), which expresses the ratio between reaction rate and convective transport, that is $D_a = kL/U$; if $D_a > 1$ the reaction is fast relative to transport, and if $D_a < 1$ transport dominates over reaction.

Deoxygenation constant due to the presence of organic load expressed in day^{-1}

In the literature, the following nomenclature is commonly used: k_r is the removal constant that includes the deoxygenation rate due to oxidation with organic matter and the removal constant due to sedimentation, $k_r = k_d + k_s$. The decay rate of carbonaceous biochemical oxygen demand developed in laboratory conditions is expressed as k_1. The decay rate of biochemical oxygen demand in natural waters is expressed as k_d. Typically, it is known that k_d or $k_1 > k_S$ [61]. Below, in Table 1, some values of the constant k_1 obtained in the field are reported.

Table 1. Reported values of kinetic constants k_1 in rivers according to different studies.

Author	Location/River	Value	Parameter
Camp [61]	Merrimack River, MA	0.01–0.1	k_1
Baca et al. [63]	Willamette River, OR	0.1–0.3	k_1
Bansal [64]	Kansas (6 rivers)	0.02–0.60	k_1
	Michigan (3 rivers)	0.56–3.37	k_1
	Truckee River, NV	0.36–0.95	k_1
	Virginia (3 rivers)	0.30–1.25	k_1
	N. Branch Potomac, WV	0.4	k_1
	South Carolina (3 rivers)	0.3–0.35	k_1
	New York (2 rivers)	0.125–0.4	k_1
	New Jersey (3 rivers)	0.2–0.23	k_1
Novotny & Krenkel [65]	Holston River, TN	0.4–1.5	k_1
Bauer et al. [66]	Chattahoochee River, GA	0.16	k_1
Greeney & Kraszewski [67]	Yampa River, CO	0.4	k_1
Crane & Malone [68]	Gray's Creek, LA	1.44	k_r
Hvitved & Jacobsen [69]	Shavad River, Denmark	0.15	k_1
	Shavad River, Denmark	0.90	k_r
Jennings et al. [70]	W. Fork Trinity River, TX	0.06–0.3	k_1
Deb & Bowers [71]	Shenandoah River, MA	0.4	k_r
Gowda [72]	Speed River, Ontario	1	k_1

Reaeration or aeration constant by solubilization of atmospheric oxygen, $k_a = k_2$ expressed in day^{-1}

A summary of reaeration or aeration constants is presented by Bowie et al. [61]; some of these equations are:

O'Connor and Dobbins: For moderate depth [73]:

$$k_a = 3.93 \times \frac{U^{0.5}}{H^{1.5}}, 0.05 \leq k_a \leq 12.22;\ 0.305 \leq H \leq 9.14;\ 0.15 \leq U \leq 0.49. \quad (26)$$

Extensive information on deoxygenation and reaeration constants, mainly as a function of geometric dimensions expressed in English units, can be found in the EPA Manual [61].

Variation in deoxygenation and reaeration constants as a function of temperature

The exponential adjustment function based on the Arrhenius–Van't Hoff equation is used, given by:

$$Q_{10} = (k_2/k_1)^{10/(T_2-T_1)}, \tag{27}$$

k_1: Reaction rate constant at temperature T_1
k_2: Reaction rate constant at temperature T_2
Q_{10}: Ratio between reaction rates for a 10 °C temperature increase.

$$k_2 = k_1 Q_{10}^{(T_2-T_1)/10}. \tag{28}$$

In general:

$$k(T) = k(T_{ref})Q_{10}^{(T_2-T_1)/10} = k(T_{ref})f(T_{ref}), \tag{29}$$

$$k(T) = k(T_{ref})Q_{10}^{(T-T_{ref})/10} = k(T_{ref})\theta^{(T-T_{ref})}. \tag{30}$$

where f is the temperature influence factor and θ is the temperature correction coefficient, whose value typically ranges between 1.016 and 1.047 for k_d and between 1.02 and 1.047 for k_a. In a specific case, the θ values used were 1.047 for deoxygenation and 1.024 for reaeration [74]. The reference temperature is usually set at 20 °C [61].

2.2. Mass Transport Equations Used in Water Pollution

The general mass transfer equation constitutes the basis for the analysis of contaminant transport in natural and artificial water bodies. This formulation integrates the main processes governing system dynamics: temporal variation in concentration, advective and diffusive transport, degradation or consumption of contaminants, and inputs from point or distributed sources.

Although under simplified conditions the model admits analytical solutions, numerical solutions offer substantial advantages by allowing a more realistic description of the phenomena involved. These include the ability to represent nonlinear or higher-order reaction kinetics, incorporate point or continuous contaminant discharges, and consider additional inputs or lateral flows of non-contaminated water at different points in the system, once the contamination process has begun at the reference point.

$$\frac{\partial C}{\partial t} + V.\nabla C = D\nabla^2 C + R \pm S. \tag{31}$$

The first term on the left-hand side of the equation represents the temporal variation in contaminant concentration, while the second term describes advective transport associated with fluid motion. On the right-hand side, the first term corresponds to diffusive transport or turbulent mixing, the second term represents the rate of contaminant consumption or degradation, and the third term incorporates the effect of an external source or sink, thus accounting for all relevant processes involved in contaminant transport within the system. In its expanded form:

$$\frac{\partial C}{\partial t} + V_x\frac{\partial C}{\partial x} + V_y\frac{\partial C}{\partial y} + V_z\frac{\partial C}{\partial z} = D_L(\frac{\partial^2 C}{\partial x^2}) + D_T(\frac{\partial^2 C}{\partial y^2}) + D_V(\frac{\partial^2 C}{\partial z^2}) + R \pm S. \tag{32}$$

Equation (32) is the basis for all developments carried out in this work; from it, the Streeter–Phelps equations and their modifications, as well as 1D, 2D, 3D, and other specific models are derived. In general, concentration is expressed in ppm; distance in m or km; time in hours; diffusion coefficients in $m^2\ s^{-1}$ or $m^2\ h^{-1}$; kinetic constants in day^{-1}; and velocities in $m\ h^{-1}$. Before performing calculations, all units must be made consistent. Supplementary equations used to estimate flow velocity, discharge, and dispersion coefficients are presented in Appendix A.

To the best of our knowledge, this study is among the first to directly compare the effectiveness of one-dimensional, two-dimensional, and three-dimensional models under similar conditions and to evaluate their performance in scenarios characterized by high hydraulic complexity and strong reactive processes.

3. Results

3.1. Determination of the Longitudinal Dispersion Coefficient

One of the most important parameters is the longitudinal dispersion coefficient. In a study conducted in the Mississippi River, dispersion experiments were carried out using the dye Rhodamine WT; sampling point 1 was located 4.3 km and point 2 at 9.6 km from the dye injection point. The river flow rate is Q = 131 m^3 s^{-1} and its average cross-sectional area is A = 1254 m^2 [44]; the corresponding data are shown in Tables 2 and 3. It should be noted that sampling must be performed downstream of the contaminant discharge point, beyond the advective zone; that is, in the "equilibrium zone".

Table 2. Tracer concentration as a function of time at sampling station 1.

t (hours)	0	1	3	5	7	9	11	13
C (mg L^{-1})	0	0.18	0.94	12.9	19	8.5	2.5	1.4
t (hours)	15	17	19	21	23	25	27	29
C (mg L^{-1})	0.93	0.71	0.51	0.4	0.29	0.21	0.16	0.13

Table 3. Tracer concentration as a function of time at sampling station 2.

t (hours)	20	20.5	22	24	25.5	27	29	31
C (mg L^{-1})	0	0.2	2.8	5.0	8.8	8.1	7.4	6.0
t (hours)	33	35	37	39	41	43	45	47
C (mg L^{-1})	4.4	3.0	2.0	1.45	1.0	0.75	0.56	0.42
t (hours)	49	51	53	55	57			
C (mg L^{-1})	0.32	0.25	0.19	0.15	0.11			

By substituting the data into Equations (15)–(17), and subsequently into Equation (14), the required parameters for calculating the longitudinal dispersion coefficient are obtained, as shown in Table 4.

Table 4. Parameters for the calculation of the longitudinal dispersion coefficient.

Location	Station 1	Station 2
X (m)	4300	9600
t (h)	8.91	31.23
σ_t^2	14.82	38.72

The mean velocity of the centroid is obtained as follows:

$$U = \frac{x_2 - x_1}{\bar{t}_2 - \bar{t}_1} = \frac{9600 - 4300}{31.23 - 8.91} = 237.4 \text{ m/h} = 6.6 \times 10^{-2} \text{ m/s}. \quad (33)$$

Finally, the dispersion coefficient is obtained as:

$$D_x = \frac{1}{2}U^2 \times \frac{\sigma_t^2(x_2) - \sigma_t^2(x_1)}{t_2 - t_1} = \frac{1}{2} \times 237.4^2 \times \frac{38.72 - 14.82}{31.23 - 8.91} = 30,173 \text{ m}^2/\text{h} = 8.4 \text{ m}^2/\text{s}. \quad (34)$$

Most of the data for running the developed program were taken from Table 2, complemented with additional data required for modeling, such as initial concentration, longitudinal, transverse, and vertical increments, among others, as shown in Table 5.

Table 5. Data for the execution of the calculation programs used.

Parameter	Value
Flow rate	131 m^3 s^{-1}
Flow area	1254 m^2
Water flow velocity (small lowland rivers)	131 × 3600/1254 => 376.076 m h^{-1}
Reaction rate constant	2.03 day^{-1} = 0.08458 h^{-1} (oxidation of ammonium to nitrite)
Longitudinal diffusion coefficient	30,173 m^2 h^{-1}
Transverse diffusion coefficient	0.6 × UC × H × 3600/50
Vertical diffusion coefficient	0.067 × UC × H × 3600/100
Study length	5300 m
Channel half-width	60 m
River depth	10.45 m
Concentration at inlet point (instantaneous and continuous input)	100 ppm
Number of points along the flow direction	10
Number of points in the transverse section	5
Number of points in the vertical section	5
Longitudinal step size	Δx = 5300/10 = 530 m
Transverse step size	Δy = 60/5 = 12 m
Vertical step size	Δz = 10.45/5 = 2.09 m
Dispersion time	14.1 h

Note: The dispersion time is obtained by dividing the channel length by the corresponding velocity, which is calculated from the flow rate and the average flow area.

The salinity value adopted in the simulations does not aim to represent a particular river system; instead, it serves as a reference condition for assessing the performance of the transport model. The methodology developed is independent of the concentration selected and can be applied to any salinity level through appropriate modification of the initial and boundary conditions.

The inlet concentration of 100 ppm was adopted as a reference value for the numerical simulations. Since the transport equations employed are linear with respect to concentration, this value only determines the scale of the results and does not affect the transport or dispersion patterns, nor the comparison among the different numerical methods analyzed. Additional equations used for the estimation of hydraulic and transport parameters employed throughout the study are provided in Appendix A.

According to Grover and Wats, the initial ranges of Chemical Oxygen Demand (COD) vary from less than 1 to 2 ppm in clean rivers, from 1 to 3 ppm in streams with normal organic loading, and from 4 to 8 ppm in moderately polluted rivers [75]. Since no experimental data are available, the simulation software has been developed to perform the analysis using any of these reference values.

3.2. One-Dimensional Transport of Soluble Contaminants

3.2.1. Method of Lines

The concentration profile of soluble contaminants is obtained from Equation (31), where the local variation in concentration, advective transport, diffusive transport in the

flow direction, the rate of consumption by reaction, and the contribution from a point source located at a specific point are considered:

$$\frac{\partial C}{\partial t} = -V_x \frac{\partial C}{\partial x} + D_L\left(\frac{\partial^2 C}{\partial x^2}\right) - kC + S. \quad (35)$$

Equation (32) can be solved in various cases, such as:

- Considering diffusive mass transport effects negligible;
- Neglecting the reaction term;
- Neglecting point source contributions;
- Considering the process under steady-state conditions.

The strategy consists of solving Equation (35) considering or not the source term S. In this case, this term is not included because its value is not known; however, if this information were available, its inclusion would not complicate the solution of the differential equation. To solve the problem, the Method of Lines is used, which consists of discretizing the spatial variables of the partial differential equation and transforming the problem into a system of ordinary differential equations, which can then be solved using appropriate numerical methods:

$$\frac{dC_i}{dt} = -V_i \frac{C_i - C_{i-1}}{\Delta x} + D_x\left(\frac{C_{i+1} - 2C_i + C_{i-1}}{\Delta x^2}\right) - kC_i \quad (36)$$

This equation is expanded for all discrete points "i" analyzed along the river segment considered in the study.

Initial and boundary conditions for pulse input:

Boundary condition 1: $C_0(0) = 0$, upstream concentration equal to zero at all times (contaminant-free water).

Initial condition: $C_1(0) > 0$; $C_2(0) = C_3(0) = \cdots = C_n(0) = 0$, contaminant-free water, except at point 1, where instantaneous discharge occurs.

Boundary condition 2: $x = L$, $dc/dx = 0$, the contaminant reaches its minimum concentration level at all times.

For the case of continuous input, it is necessary to modify boundary condition 1 and the initial condition.

Boundary condition 1: $C_0(0) > 0$, upstream concentration equal to zero at all times (water free of contaminants).

Initial condition: $C_1(0) = 0$; $C_2(0) = C_3(0) = \cdots = C_n(0) = 0$, water free of contaminants, except at point 1, where the instantaneous discharge occurs.

Contaminant removal rate

The effectiveness (η) in contaminant removal in river flow is used in environmental engineering to evaluate how efficiently a chemical, biological, or physical reaction occurs within a porous medium (such as riverbed sediment) or in a "transient storage" zone (such as stagnant water in pools or the hyporheic zone), compared to its maximum potential rate. That is, the removal rate is limited by diffusion and reaction divided by the removal rate if the reaction were not diffusion limited.

From Equation (32), an analytical solution is obtained [76], which is mainly used to determine the contaminant removal effectiveness factor:

$$C(x,t) = \frac{C_0 U \Delta t}{\sqrt{4\pi D_L t}} exp\left[-\frac{(x - U \times t)^2}{4 D_L t}\right] \times exp(-kt), \quad (37)$$

$C(x,t)$: Concentration as a function of time and distance (ppm)

C_0: Pulse concentration (ppm)

U: Mean flow velocity (m h^{-1})
D_L: Diffusion coefficient (m^2 h^{-1})
x: Distance (m)
t: Duration time of the contamination event (h)
Δt: Pulse duration period (h)
k: Reaction rate constant (h^{-1}).
The mass flux $J(t)$ at the outlet section is given by:

$$J(t) = U \times C(L,t), \tag{38}$$

$$M_{out} = \int_0^\infty J(t)dt = \int_0^\infty U \times C(L,t)dt, \tag{39}$$

$$\eta = 1 - \frac{M_{out}}{M_{injected}}, \tag{40}$$

$$\eta = 1 - \frac{\int_0^\infty \frac{C_0 U \Delta t}{\sqrt{4\pi D_L t}} exp\left[-\frac{(x-U\times t)^2}{4D_L t}\right] \times exp(-kt)dt}{C_0}. \tag{41}$$

Simplifying:

$$\eta = 1 - \int_0^\infty \frac{U\Delta t}{\sqrt{4\pi D_L t}} exp\left[-\frac{(x - U \times t)^2}{4D_L t}\right] \times exp(-kt)dt = 1 - U\Delta t \times I. \tag{42}$$

Scheme of the one-dimensional transport process

Figure 1 shows the scheme of one-dimensional contaminant transport, where it is observed that both the velocity profile and the concentration profile tend to be turbulent, that is, independent of the river width and depth. Therefore, the one-dimensional transport assumption is valid, and all the previous developments are applicable. Likewise, it must be considered that along the studied segment, the flow rate remains constant; however, based on the channel configuration, variations in width are observed, which implies variations in velocity. Therefore, it is possible to introduce a variable velocity within the mass balance scheme given by Equation (36).

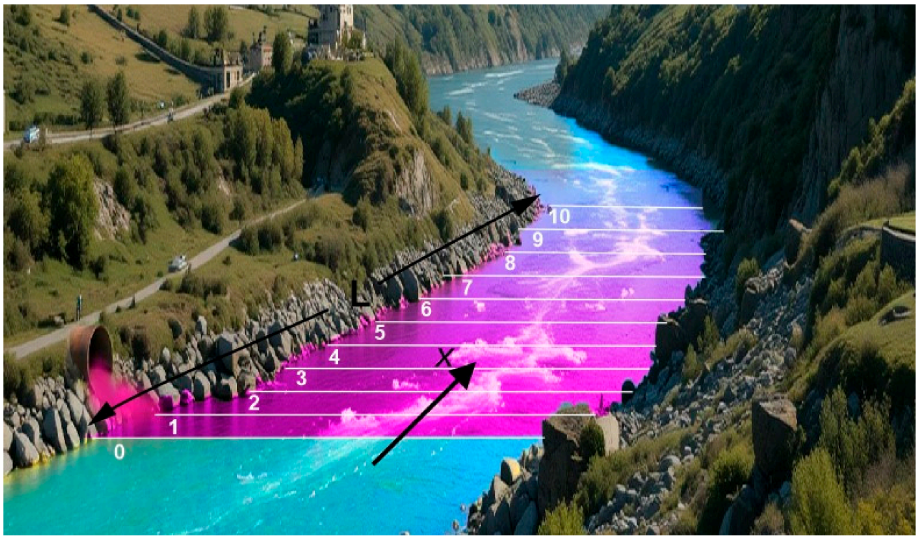


Figure 1. Scheme of one-dimensional contaminant transport.

In Figure 2a, the contaminant concentration profile as a function of time is shown for each segment of the studied river reach, considering a pulse-type contaminant input at a

given point of the channel. In turn, Figure 2b presents the contaminant concentration profile as a function of time for each segment of the river reach under a continuous contaminant input condition.

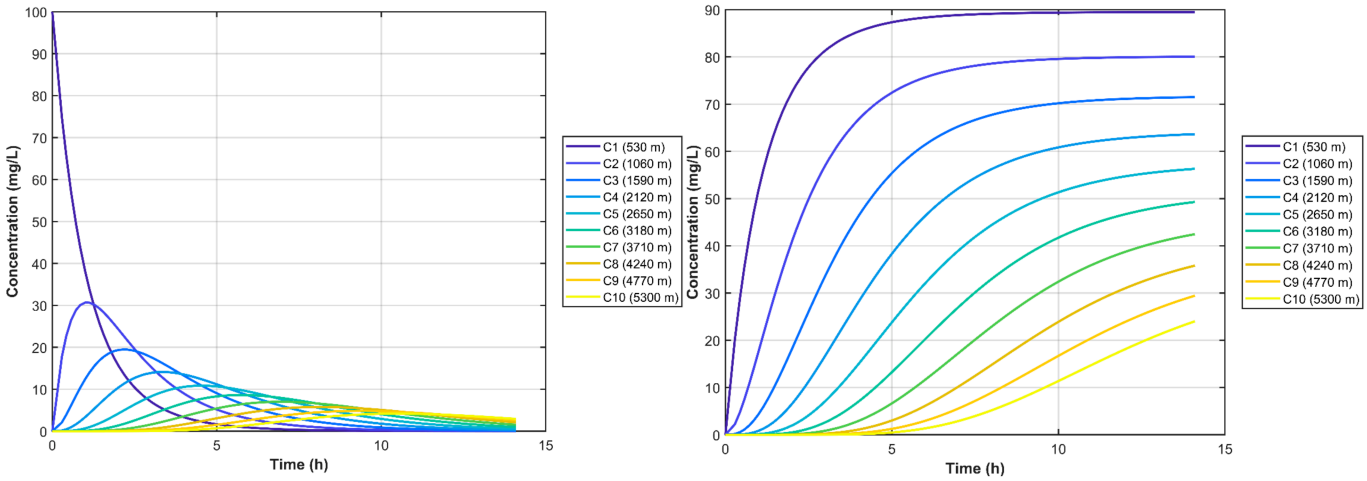


Figure 2. Contaminant concentration profile as a function of time using the Method of Lines for (**a**) Pulse-type input, and (**b**) Continuous input.

To verify the correct implementation of the numerical model, the results obtained using the Method of Lines, Equation (36) were compared with the analytical solution of Equation (37) for the one-dimensional case of pulse contaminant transport. At a simulation time of 1 h, the analytical solution predicted a maximum concentration of 31 ppm, whereas the numerical solution yielded a value of 30.6 ppm, corresponding to an approximate relative difference of 1.3%. This close agreement confirms the accuracy of the numerical scheme employed. It should be noted that analytical solutions are generally limited to simplified cases, whereas the numerical methods developed in this study allow the analysis of more complex scenarios, including multiple contamination sources, diffuse pollutant discharges, and variable boundary conditions, for which closed-form analytical solutions are generally unavailable.

3.2.2. Explicit Finite Difference Method

It consists of transforming differential Equation (32) into a system of linear algebraic equations (if the kinetics is first order) and nonlinear systems (if the kinetics is of order "n"), with the possibility of calculating each of the variables (concentrations as a function of time and distance) point by point. The method is simple to implement; however, it may become computationally expensive for fine discretization's, although it remains widely used because of its simplicity. The discretized scheme is as follows:

$$\frac{C_{i,j+1} - C_{i,j}}{\Delta t} + V_i \frac{C_{i,j} - C_{i-1,j}}{\Delta x} - D_L \frac{C_{i+1,j} - 2C_{i,j} + C_{i-1,j}}{\Delta x^2} + kC_{i,j} = 0. \quad (43)$$

Rearranging Equation (43):

$$C_{i,j+1} = \left(1 - \frac{V_i \Delta t}{\Delta x} - \frac{2D_L \Delta t}{\Delta x^2} - k\Delta t\right) C_{i,j} + \left(\frac{V_i \Delta t}{\Delta x} + \frac{D_L \Delta t}{\Delta x^2}\right) C_{i-1,j} + \frac{D_L \Delta t}{\Delta x^2} C_{i+1,j}. \quad (44)$$

In this scheme, concentration is computed at each spatial location and time step; there is also the possibility of varying the velocity at each point. All terms on the right-hand side of Equation (44) must be known, and stability criteria of the algebraic system must also be satisfied.

The following change in variables is performed:

$$A_i = 1 - \frac{V_i \Delta t}{\Delta x} - \frac{2D_L \Delta t}{\Delta x^2} - k\Delta t$$

$$B_i = \frac{V_i \Delta t}{\Delta x} + \frac{D_L \Delta t}{\Delta x^2}$$

$$D = \frac{D_L \Delta t}{\Delta x^2}$$

With these changes, Equation (37) is transformed into:

$$C_{i,j+1} = A_i C_{i,j} + B_i C_{i-1,j} + D C_{i+1,j} \tag{45}$$

This system applies both for pulse-type and continuous contaminant input. In the case of pulse input $C_{0,j} = 0$, j = 0, 1, 2, 3, . . ., n; $C_{1,0} \neq 0$ and all other initial concentrations equal to 0. In the case of continuous input, $C_{i,0} = 0$, i = 1, 2, 3, . . ., m; $C_{0,j} \neq 0$, j = 0, 1, 2, 3, . . ., n.

Using the data from Table 5 for a time of 3 h, the contaminant concentration profile is obtained in different segments of the river reach and at different times, as shown in Figure 3.

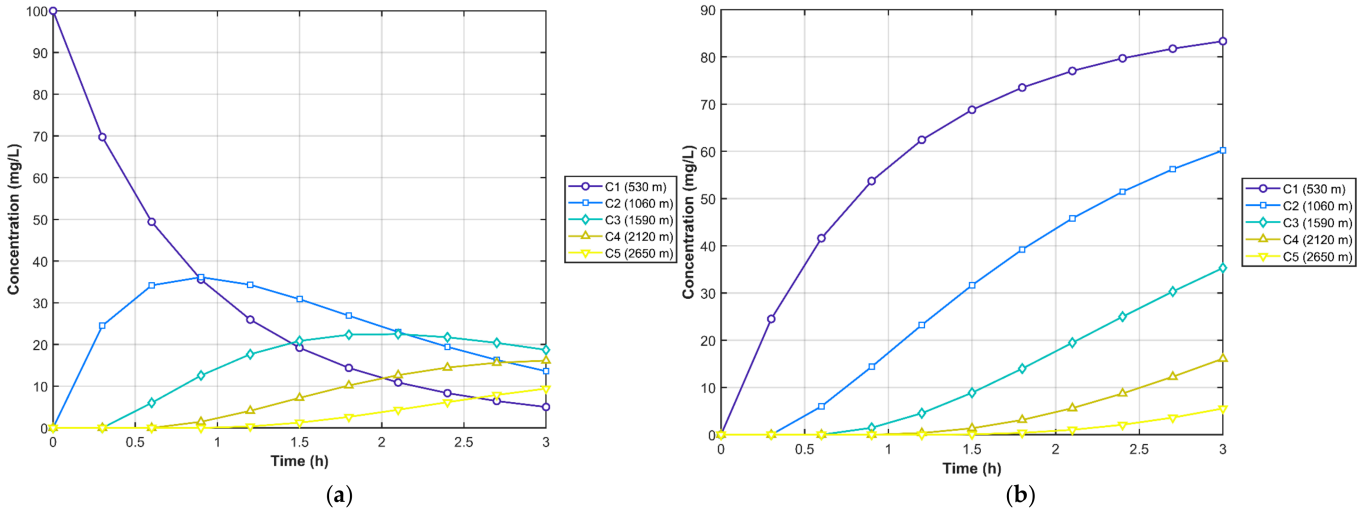


Figure 3. Contaminant concentration profile as a function of time using the explicit finite difference method considering the first 5 channel segments for (**a**) Pulse-type input, and (**b**) Continuous input.

Due to the limited capacity of the software, the program was executed for a total of three hours; for this time, both the Method of Lines and the explicit finite difference method show matching values.

3.2.3. Implicit Finite Difference Method

The discretization of Equation (35) using the implicit finite difference method leads to a system of linear algebraic equations, under the assumptions of first-order kinetics and a velocity that, although it may be considered variable, is independent of the velocity profile.

$$\frac{C_{i,j+1} - C_{i,j}}{\Delta t} + V_i \frac{C_{i,j+1} - C_{i-1,j+1}}{\Delta x} - D_L \frac{C_{i+1,j+1} - 2C_{i,j+1} + C_{i-1,j+1}}{\Delta x^2} + kC_{i,j+1} = 0. \tag{46}$$

Rearranging:

$$\left(1 + \frac{V_i \Delta t}{\Delta x} + \frac{D_L \Delta t}{\Delta x^2} + k\Delta t\right) C_{i,j+1} - \left(\frac{V_i \Delta t}{\Delta x} + \frac{D_L \Delta t}{\Delta x^2}\right) C_{i-1,j+1} - C_{i,j} - \frac{D_L \Delta t}{\Delta x^2} C_{i+1,j+1} = 0. \tag{47}$$

$$A_i = 1 + \frac{V_i \Delta t}{\Delta x} + \frac{2D_L \Delta t}{\Delta x^2} + k\Delta t,$$

$$B_i = \frac{V_i \Delta t}{\Delta x} + \frac{D_L \Delta t}{\Delta x^2},$$

$$D_i = \frac{D_L \Delta t}{\Delta x^2},$$

$$A_i C_{i,j+1} - B_i C_{i-1,j+1} - C_{i,j} - DC_{i+1,j+1} = 0. \quad (48)$$

Equation (48) is a tridiagonal matrix system, whose solution is obtained row by row; that is, it allows obtaining all concentration values along the river or channel for each time step. For time step 1, the matrix equation obtained is $D_i = \frac{D_L \Delta t}{\Delta x^2}$.

The value of M can take one of the following values: $C_{1,0}$ for pulse input and $B_1 C_{0,1}$ for continuous inflow. It is also possible to solve simultaneously for multiple time steps; however, it is necessary to rewrite the system, which in this case becomes a block tridiagonal system, where each matrix element is another matrix and the variables, as well as the independent terms, become vectors. In both cases—row-by-row calculation or global calculation—the system is solved using the Thomas algorithm.

The calculation was carried out using the data from Table 5 for the entire interval of 5300 m and for a time of 3 h, and for pulse-type input conditions, the reported data are shown in Figure 4a.

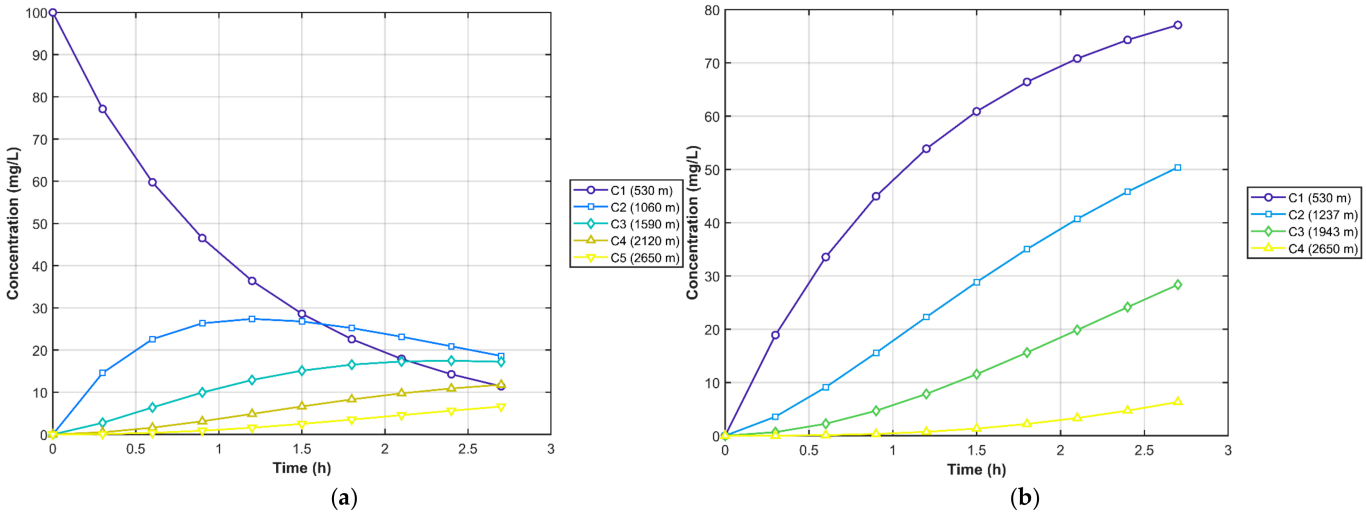


Figure 4. Contaminant concentration profile as a function of time using the implicit finite difference method for (**a**) Pulse-type, and (**b**) Continuous contaminant input.

Figure 4b shows the concentration profiles obtained with the implicit finite-difference algorithm for a distance of 5300 m and 3 h of contaminant travel, when the contaminant input is continuous as a result of a constant contaminant flow into a water stream that was initially contaminant-free.

3.3. Two-Dimensional Transport of Soluble Contaminants

In this case, the same techniques used in the 1D model are also applied, that is, transforming Equation (49) into a system of ordinary differential equations or into a system of linear algebraic equations, since the kinetics is first order.

$$\frac{\partial C}{\partial t} + V_x \left(\frac{\partial C}{\partial x} \right) = D_x \left(\frac{\partial^2 C}{\partial x^2} \right) + D_y \left(\frac{\partial^2 C}{\partial y^2} \right) - kC. \quad (49)$$

For turbulent flow, the velocity is independent of the width of the channel or river; the discretization of (47) using the implicit method leads to:

$$\frac{dC_{i,j}}{dt} = -V_i\left(\frac{C_{i,j+1} - C_{i-1,j+1}}{\Delta x}\right) + D_L\left(\frac{C_{i+1,j+1} - 2C_{i,j+1} - C_{i-1,j+1}}{\Delta x^2}\right) + D_T\left(\frac{C_{i,j+1} - 2C_{i,j} - C_{i,j-1}}{\Delta y^2}\right) - kC_{i,j+1}. \quad (50)$$

For flows without predominant turbulence and with regular cross-sectional dimensions of the studied channel, the velocity can be written as a function of the semi-width of the river, that is:

$$V_x = V_{max}\left[1 - \left(y/W\right)^2\right]. \quad (51)$$

Figure 5 illustrates the dispersion process and highlights concentration variations in both the longitudinal and transverse directions. Therefore, the solution of differential Equation (49) is much more feasible using numerical techniques, for which the discretization of Equations (49) and (50) is performed:

$$\frac{dC_{i,j}}{dt} = -V_{max}\left[1 - \left(j\Delta y/W\right)^2\right]\left(\frac{C_{i,j+1} - C_{i-1,j+1}}{\Delta x}\right) + D_L\left(\frac{C_{i+1,j+1} - 2C_{i,j+1} - C_{i-1,j+1}}{\Delta x^2}\right) + D_T\left(\frac{C_{i,j+1} - 2C_{i,j} - C_{i,j-1}}{\Delta y^2}\right) - kC_{i,j+1}. \quad (52)$$

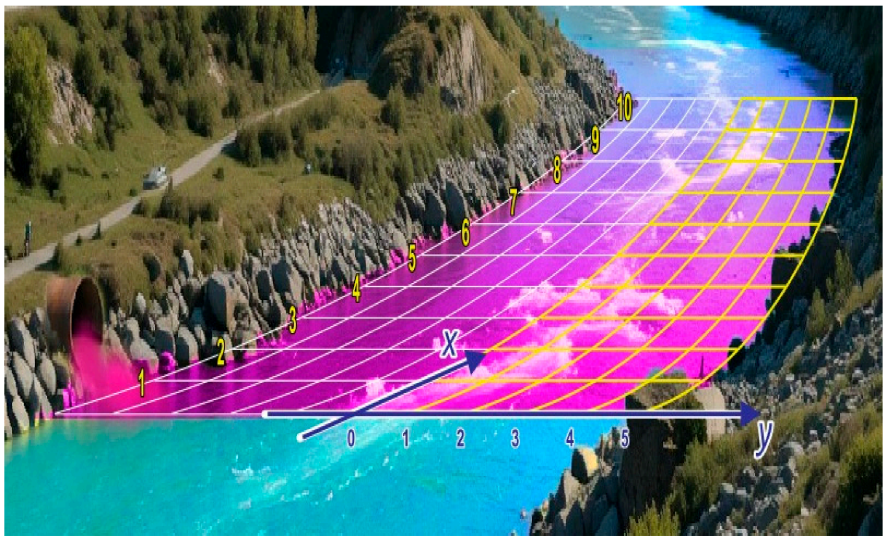


Figure 5. Scheme of two-dimensional contaminant transport.

The initial conditions, by dividing the semi-width into 5 parts and the length into 10 parts, lead to the generation of 60 ordinary differential equations and 57 auxiliary equations.

Initial condition for pulse-type input: $C_{0,j}(0) = 0$; $j = 0 \ldots 5$ (upstream water is contaminant-free at all times), and at the contaminant input point: $C_{1,j}(0) > 0$ (in this case assumed 100 ppm); $C_{i,j}(0) = 0; i = 2 \ldots 10; j = 0 \ldots 5$ (all downstream points are initially contaminant-free).

Initial condition for continuous input: $C_{0,j}(0) > 0; j = 0 \ldots 5$ upstream water is contaminated at all times (in this case 100 ppm), and downstream $C_{i,j}(0) = 0; i = 1 \ldots 10; j = 0 \ldots 5$ at all times.

The boundary conditions at any time $t > 0$ are the same for both cases: pulse input and continuous input.

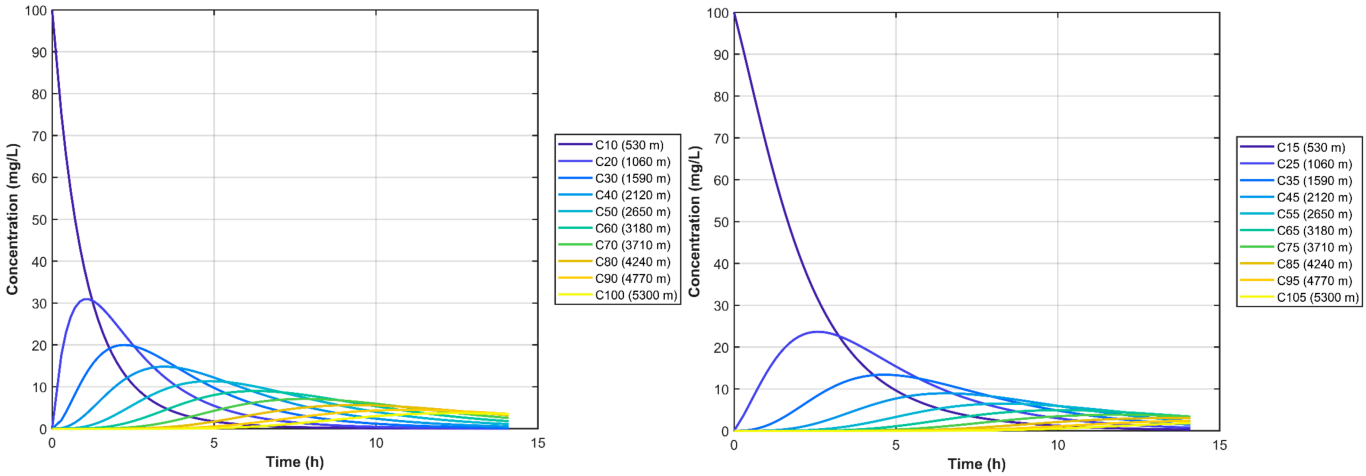
$y = 0\ \frac{dC_{i,0}}{dy} = 0\ \forall\ i = 2 \ldots 10$ (maximum concentration condition)

$y = W\ \frac{dC_{i,5}}{dy} = 0\ \forall\ i = 2 \ldots 10$ (minimum concentration condition)

$x = L\ \frac{dC_{10,j}}{dx} = 0\ \forall\ i = 2 \ldots 10$ (minimum concentration at the final stage)

For the execution of the developed computational program, data from Table 5 are used, and the following concentration profiles as a function of time are obtained for each

segment of the selected channel or river, for pulse-type input. Since a very large family of curves is obtained (60 curves), Figure 6 shows the family of curves along the symmetry axis of the channel and at the edge for pulse-type input.

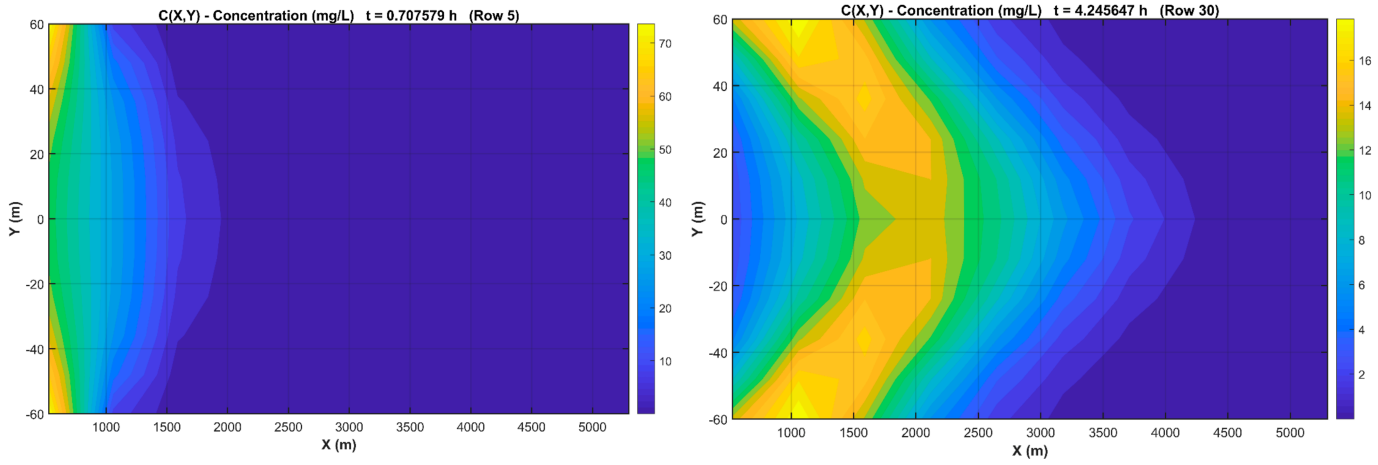


(**a**) (**b**)

Figure 6. Concentration profile for pulse-type contaminant input at (**a**) Central axis (y = 0: transverse symmetry axis), and (**b**) Concentration profile at the channel edge (y = W).

The concentration is identified with two subscripts; the first subscript represents the position with respect to x, while the second subscript represents the position with respect to y; for example, C80 means position 8 with respect to the *x*-axis (distance of 4240 m) and at y = W, that is, at the edge (y = 60 m). The same nomenclature is followed for the case of continuous input.

In Figure 7 the concentration profiles are shown along the bed of 5300 m and the width of 120 m for four different times for pulse-type input.



(**a**) (**b**)

Figure 7. Longitudinal and transverse concentration profile of soluble contaminants at (**a**) t = 0.71 h, (**b**) t = 4.25 h.

Figure 8 shows representative concentration profiles along the channel centerline (y = 0) and at the channel edge (y = W) for continuous upstream contaminant input under initially contaminant-free conditions.

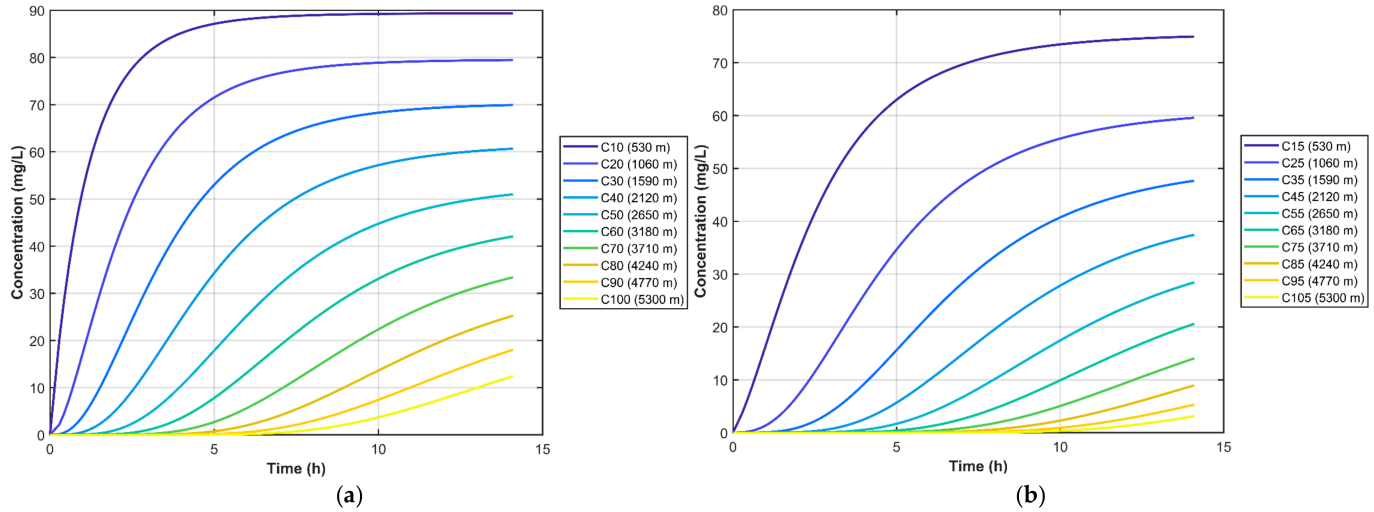


Figure 8. Concentration profile for continuous contaminant input at (**a**) the central axis (y = 0: transverse symmetry axis) along the channel, and (**b**) the channel edge (y = 60).

In Figure 9 the concentration profiles are shown along the bed of 5300 m and the width of 120 m for four different times for continuous input.

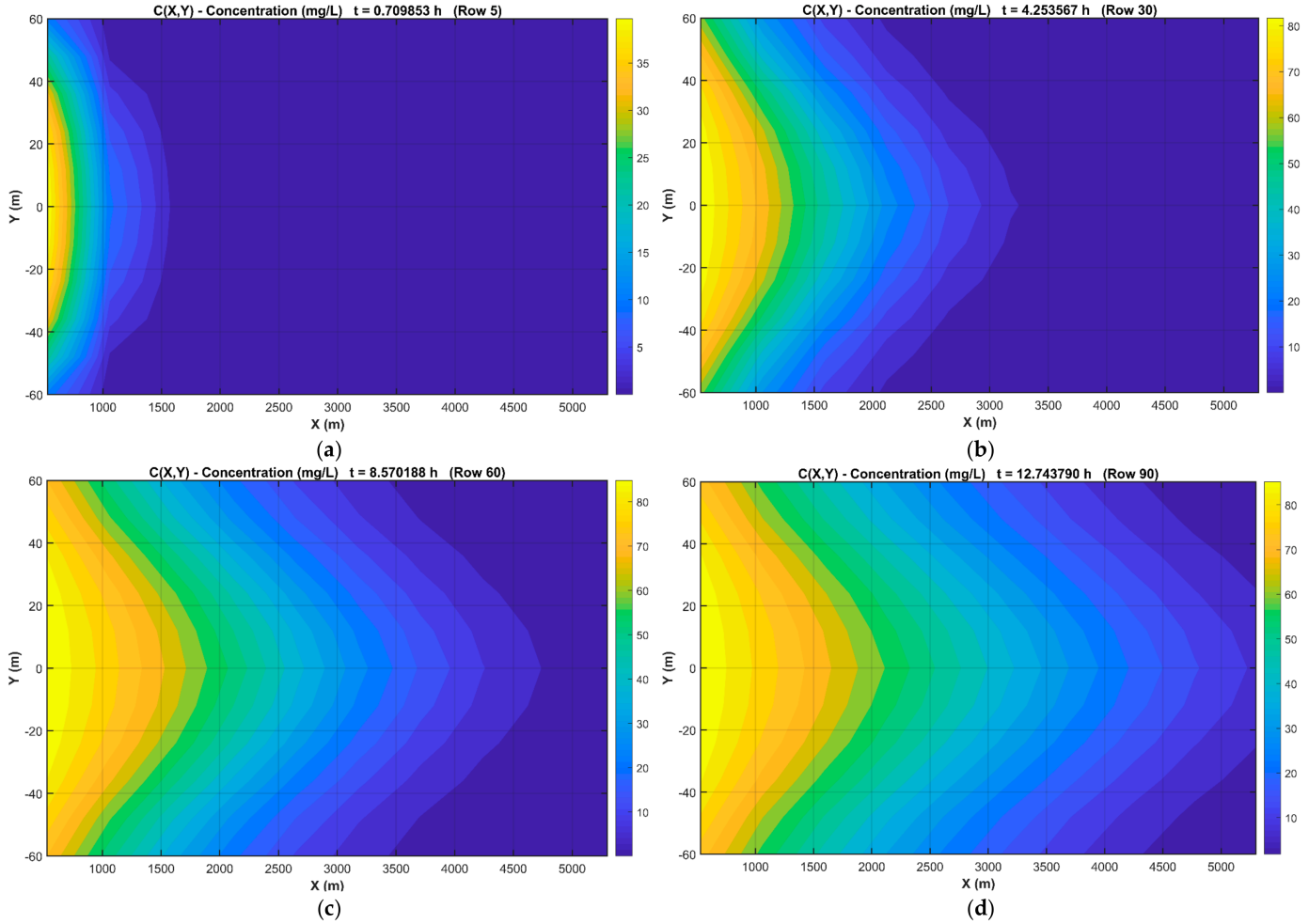


Figure 9. Longitudinal and transverse concentration profile of soluble contaminants at (**a**) t = 0.71 h, (**b**) t = 4.25 h, (**c**) t = 8.57 h, and (**d**) t = 12.74 h.

3.4. Three-Dimensional Transport of Soluble Contaminants

Contaminant transport is assumed to occur under near-laminar flow conditions with a velocity profile dependent on channel width and depth. Consequently, dispersion develops in the longitudinal, transverse, and vertical directions, as described by Equations (53) and (54). Contaminant mass balance:

$$\frac{\partial C}{\partial t} + V_x \frac{\partial C}{\partial x} = D_x\left(\frac{\partial^2 C}{\partial x^2}\right) + D_y\left(\frac{\partial^2 C}{\partial y^2}\right) + D_y\left(\frac{\partial^2 C}{\partial z^2}\right) - kC. \tag{53}$$

The velocity equation depends on the channel half-width and depth, as described by Equation (54) and illustrated in Figure 10:

$$V_x = V_{max}\left[H^2\left(1 - \left(z/H\right)^2\right) \times W^2\left(1 - \left(y/W\right)^2\right)\right]. \tag{54}$$

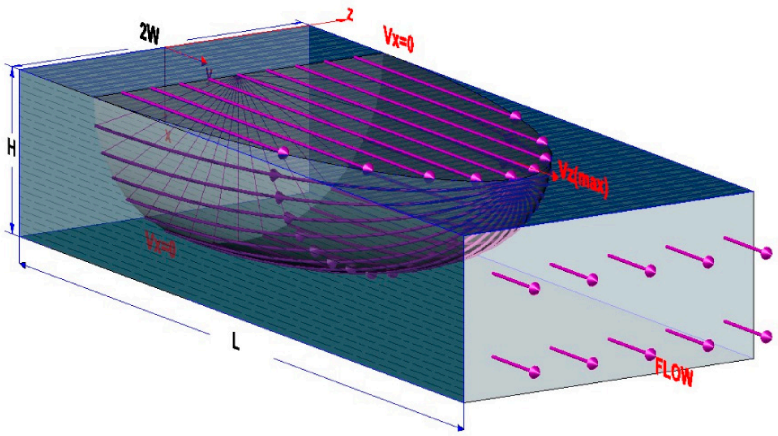


Figure 10. Velocity profile scheme.

Figure 11 shows a schematic representation of three-dimensional contaminant transport and the computational grid used to visualize the numerical solution of the partial differential Equation (53).

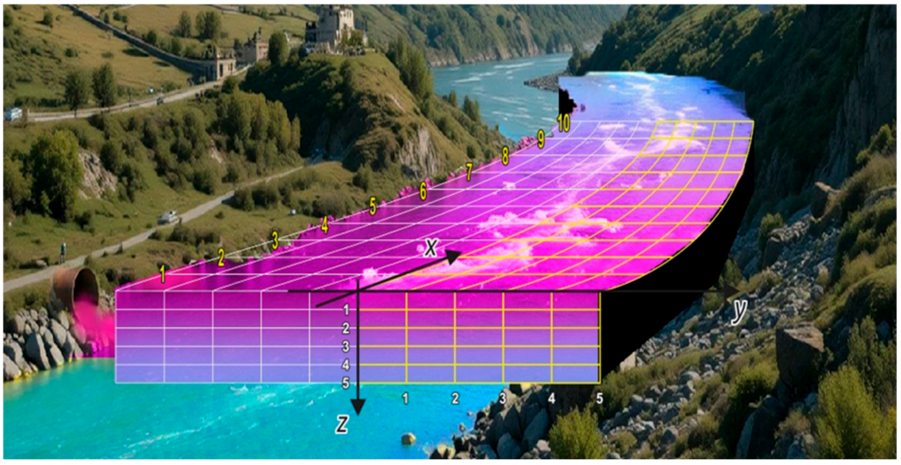


Figure 11. Three-dimensional contaminant transport scheme.

The discretization of Equation (53) yields:

$$\frac{dC_{i,j,k}}{dt} = -V_i\left(\frac{C_{i,j,k} - C_{i-1,j,k}}{\Delta x}\right) + D_L\left(\frac{C_{i+1,j,k} - 2C_{i,j,k} + C_{i-1,j,k}}{\Delta x^2}\right) + D_T\left(\frac{C_{i,j+1,k} - 2C_{i,j,k} + C_{i,j-1,k}}{\Delta y^2}\right) + D_V\left(\frac{C_{i,j,k+1} - 2C_{i,j,k} + C_{i,j,k-1}}{\Delta z^2}\right) - kC_{i,j,k}. \tag{55}$$

In this case, the partial differential Equation (53) has also been transformed into a system of ordinary differential equations, whose graphical scheme allows identification of each discretized point (i, j, k).

For the modeling, the domain is discretized as follows: the longitudinal axis x is divided into 10 segments (i = 1, 2, . . ., 10), the transverse axis y into 5 segments (j = 0, 1, . . ., 5), and the vertical axis z into 5 segments (k = 0, 1, . . ., 5). The resulting discretization provides sufficient spatial resolution to capture the three-dimensional transport dynamics analyzed in this study.

The initial and boundary conditions for pulse-type contaminant input, inferred from the previous schematic, are:

Initial condition: For $t = 0, \forall y \geq 0 \; \forall z \geq 0$.

$C_{0,j,k} = 0 \; \forall t \geq 0 \; \forall y \geq 0 \; \forall y \geq 0$ (The upstream contaminant concentration is zero, that is, contaminant-free); $t = 0 \; C_{1,j,k} \neq 0, \forall y \geq 0 \; \forall z \geq 0$ (Pulse-type contaminant input); $t \leq 0 \; C_{i,j,k} = 0 \; i = 2 \ldots 10 \; \forall y \geq 0 \; \forall z \geq 0$ (all downstream points at the initial time are contaminant-free); in all cases $x \leq L \; y \leq W \; z \leq H$, therefore, $i = 2 \ldots 10 \; j = 0 \ldots 5 \; k = 0 \ldots 5$ (arbitrarily established for this case).

$y = 0 \; \frac{\partial C_{i,0,k}}{\partial y} = 0 \; \forall x \geq 0 \; \forall z \geq 0 \; \forall t > 0$ Boundary condition 1

$y = \pm W \; \frac{\partial C_{i,5,k}}{\partial y} = 0 \; \forall x \geq 0 \; \forall z \geq 0 \; \forall t > 0$ Boundary condition 2

$z = 0 \; \frac{\partial C_{i,j,0}}{\partial z} = 0 \; \forall x \geq 0 \; \forall y \geq 0 \; \; \forall t > 0$ Boundary condition 3

$z = H \; \frac{\partial C_{i,j,5}}{\partial z} = 0 \; \forall x \geq 0 \; \forall y \geq 0 \; \forall t > 0$ Boundary condition 4

$z = L \; \frac{\partial C_{10,j,5}}{\partial x} = 0 \; \forall y \geq 0 \; \forall z \geq 0 \; \forall t > 0$ Boundary condition 5

Figure 12 shows an enlarged schematic of Figures 10 and 11, representing the length, half-width, and depth of the river.

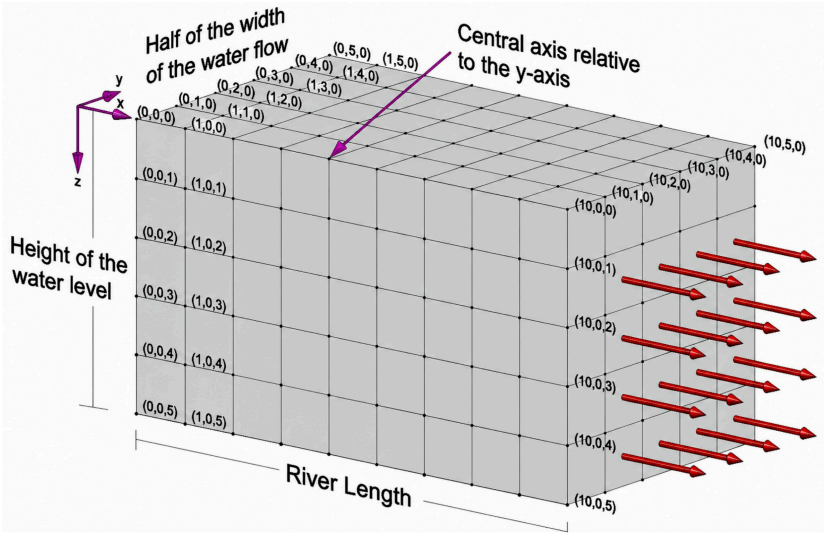


Figure 12. Grid scheme for three-dimensional transport.

For continuous input conditions, only the initial condition is slightly modified, while boundary conditions remain unchanged. For visualization purposes, representative concentration profiles corresponding to key spatial locations are presented:

- Central axis at the free surface (y = 0, z = 0), Figure 13a;
- Channel edge at the free surface (y = W, z = 0), Figure 13b;
- Channel bed at the central axis (y = 0, z = H), Figure 13c.

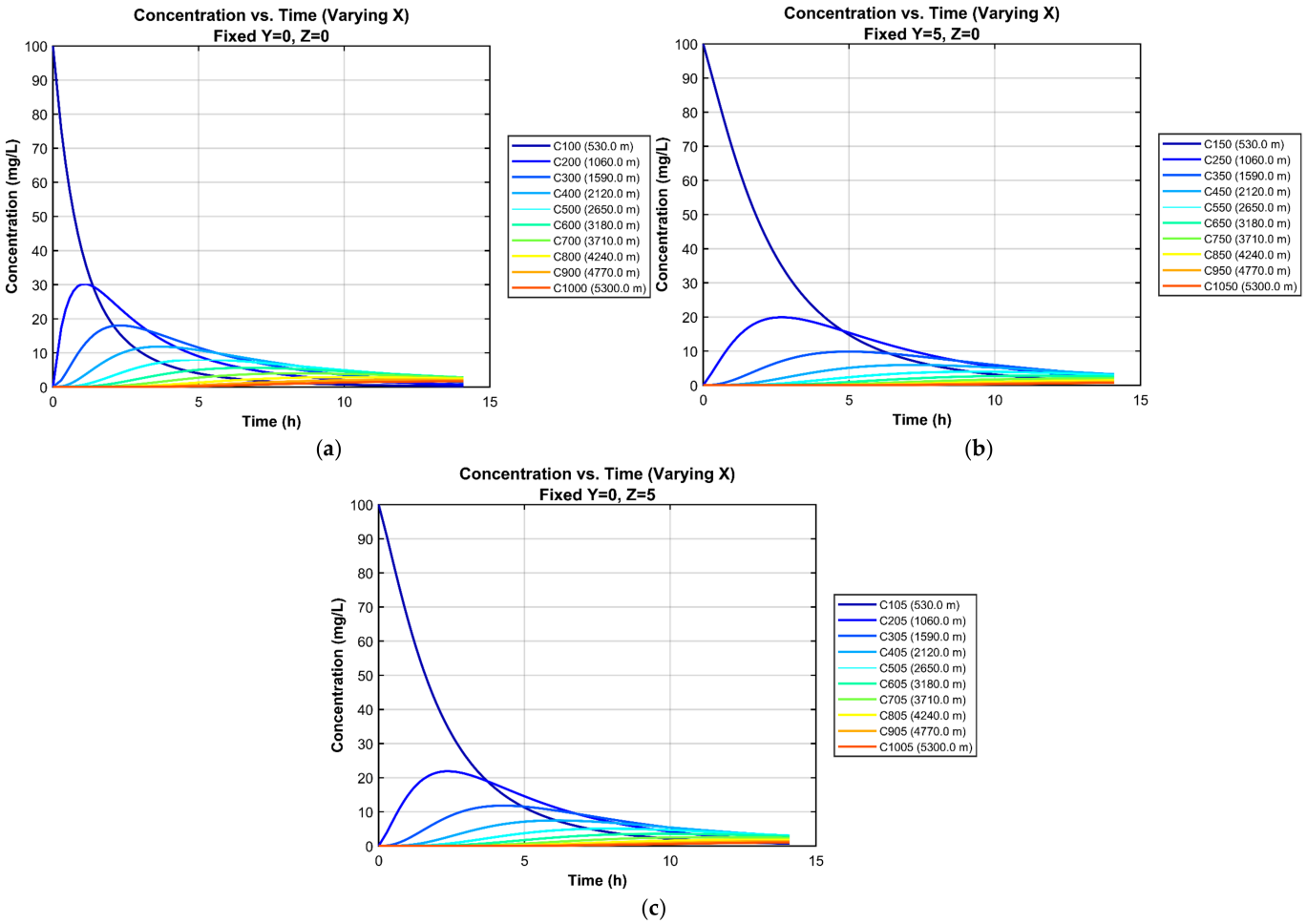


Figure 13. Concentration profile for pulse input at (**a**) y = 0, z = 0, (**b**) y = W, z = 0, and (**c**) y = 0, z = H.

Representative concentration profiles at selected locations are presented in Figure 13.

Figure 14 present contour and surface plots of longitudinal and vertical concentration profiles at y = 0 over a distance of 5300 m for different times, considering pulse input.

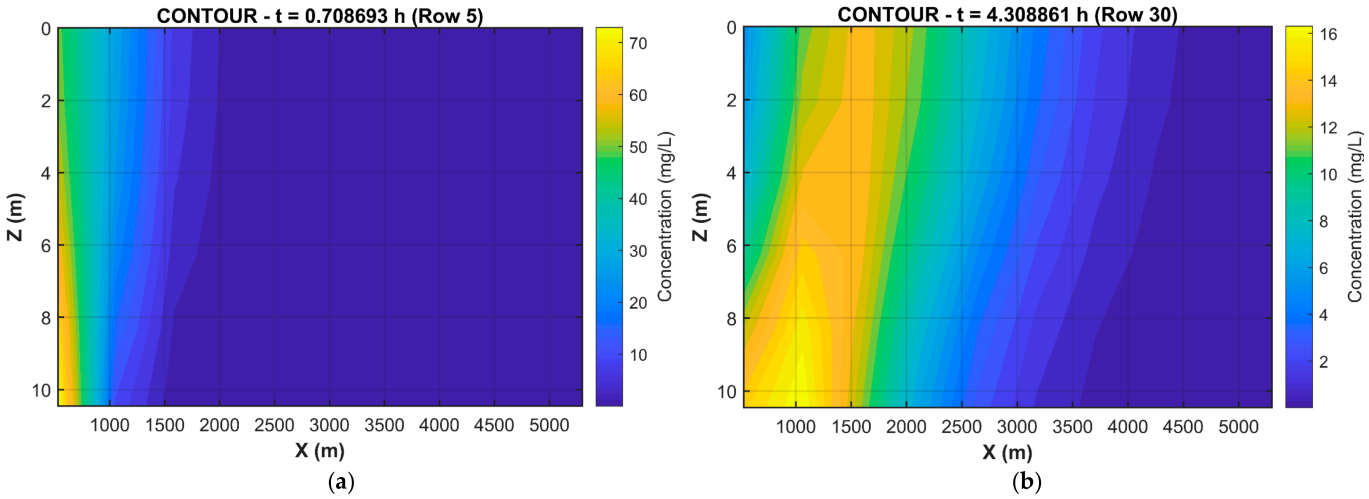


Figure 14. *Cont.*

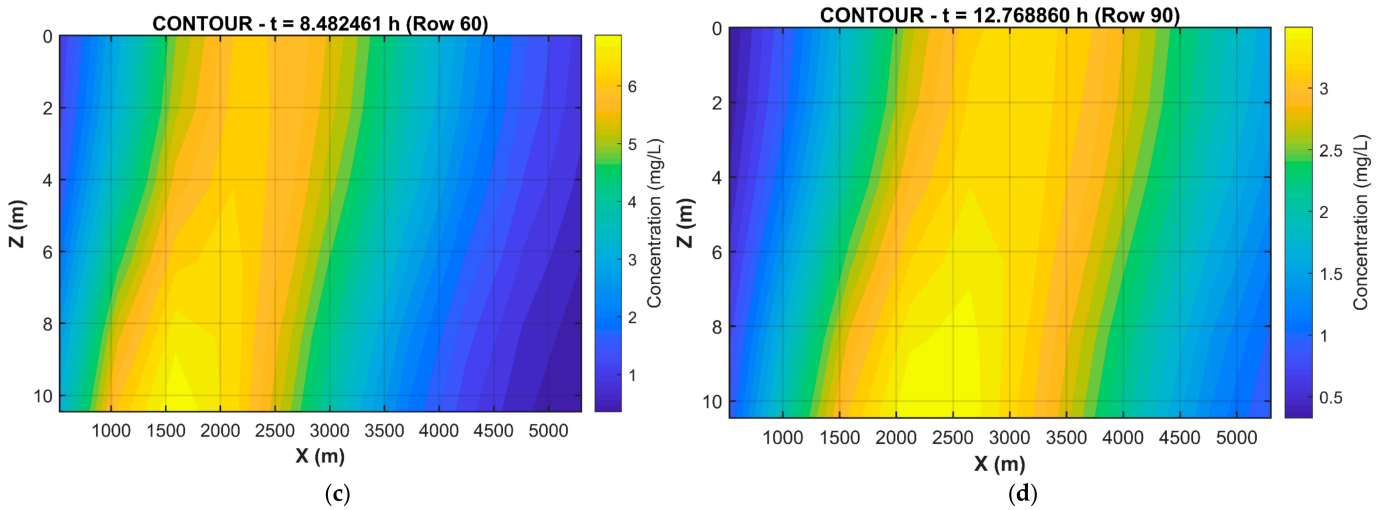


Figure 14. Contour and surface plots of longitudinal and vertical concentration profiles at y = 0 over a distance of 5300 m considering pulse input for (**a**) t = 0.72 h, (**b**) t = 4.24 h, (**c**) t = 8.48 h, and (**d**) t = 12.77 h.

Figure 15 presents a subfamily of concentration profiles obtained from the continuous contaminant input process along a distance of 5300 m as a function of time under different spatial conditions. Figure 15a shows the concentration profiles evaluated along the central axis of the channel (y = 0) and at the free surface of the fluid (z = 0). Figure 15b illustrates the concentration profiles corresponding to the channel boundary (y = W) and the free surface (z = 0). Finally, Figure 15c depicts the concentration profiles evaluated at the channel boundary (y = W) and at the channel depth (z = H). Together, these profiles describe the temporal and spatial evolution of contaminant concentration throughout the study domain under continuous contaminant discharge conditions.

Figure 16 shows contour and surface plots of the contaminant concentration profile at a distance of 5300 m, along the central axis (y = 0), as a function of height for each time step, under continuous contaminant input.

Additional profiles can be obtained by selecting the corresponding points from the computed dataset.

The three-dimensional model developed represents the most general formulation considered in this study, as it allows the simultaneous description of longitudinal, transverse, and vertical variations in contaminant concentration. From a computational perspective, its implementation using the Method of Lines leads to a system of approximately 360 coupled ordinary differential equations. The two-dimensional and one-dimensional models can be interpreted as particular cases derived from this general formulation through appropriate simplifications of the geometry and the spatial variables considered. This hierarchical structure provides a flexible framework for analyzing different contaminant transport scenarios while maintaining mathematical and numerical consistency across the various levels of modeling.

The results presented in the 1D, 2D, and 3D models highlight the importance of understanding how dispersion and reaction processes, as well as boundary and input conditions, influence the dynamics of contaminant transport in aquatic environments. In Section 3.2, the determination of the longitudinal dispersion coefficient reveals that mixing and turbulence within the river promote rapid homogenization of concentrations, which is essential for the natural self-purification capacity of the water body. The review of the Lines method in Section 3.3 demonstrates that, although this approach simplifies the problem through spatial discretization, it accurately captures the combined effects of advection, diffusion, and reaction, emphasizing that dispersion contributes significantly to contaminant

dilution and, consequently, to the recovery of water quality. Finally, in Section 3.4, the three-dimensional modeling shows that transverse and vertical variations in concentration cannot be neglected in contexts where physical and biological processes interact across different spatial scales, underscoring the need for integrated and higher-resolution approaches for effective environmental management. Taken together, these findings support the idea that contaminant transport is not merely a process of physical movement, but rather a complex interaction among hydraulic dynamics, reaction mechanisms, and dispersion processes, which collectively determine the system's capacity for self-purification and the maintenance of healthy ecological conditions.

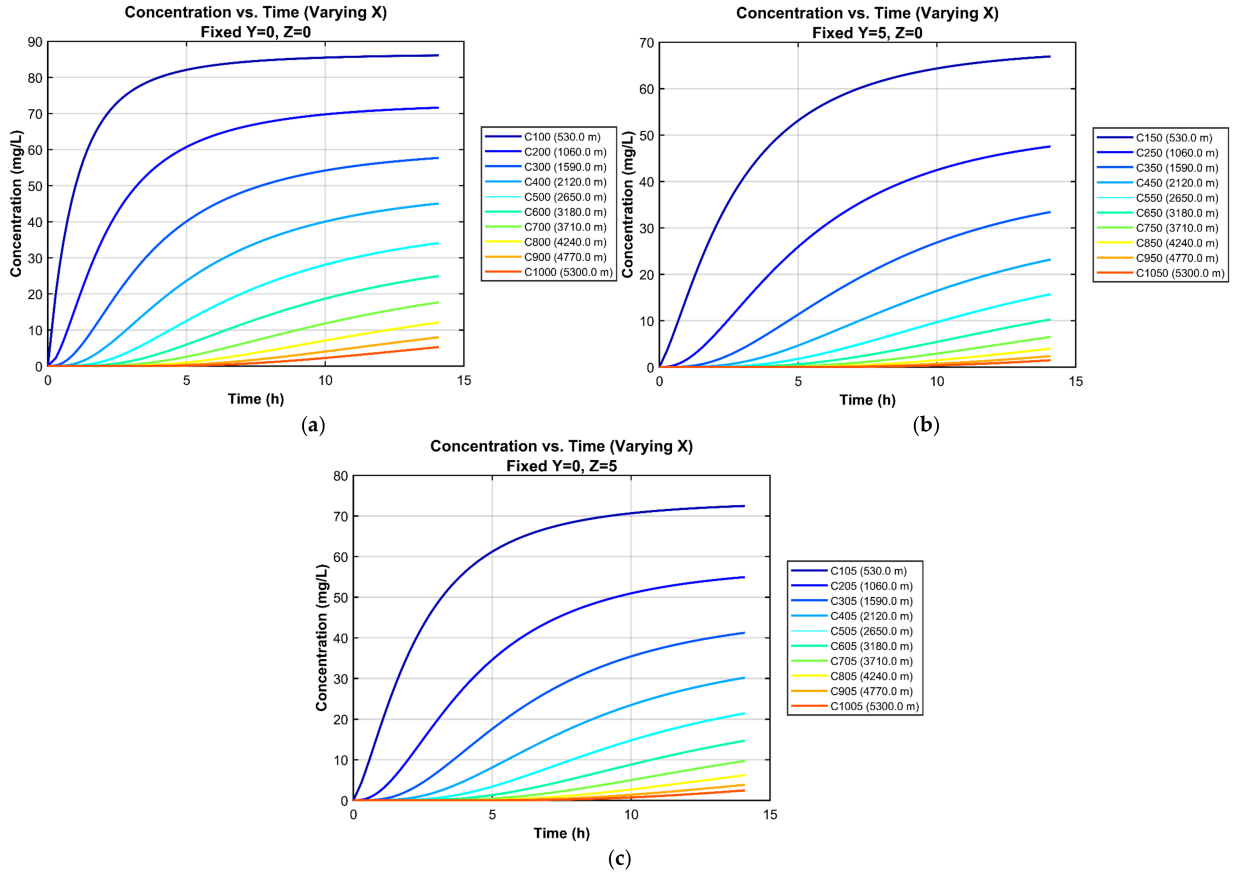


Figure 15. Concentration profile for continuous input at (**a**) y = 0, z = 0, (**b**) y = W, z = 0, and (**c**) y = W, z = H.

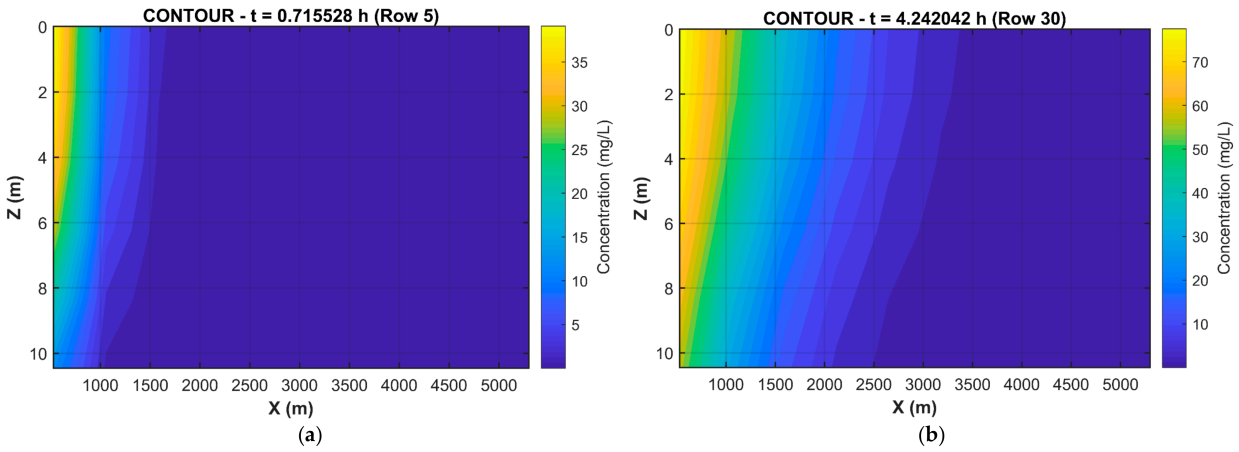


Figure 16. *Cont.*

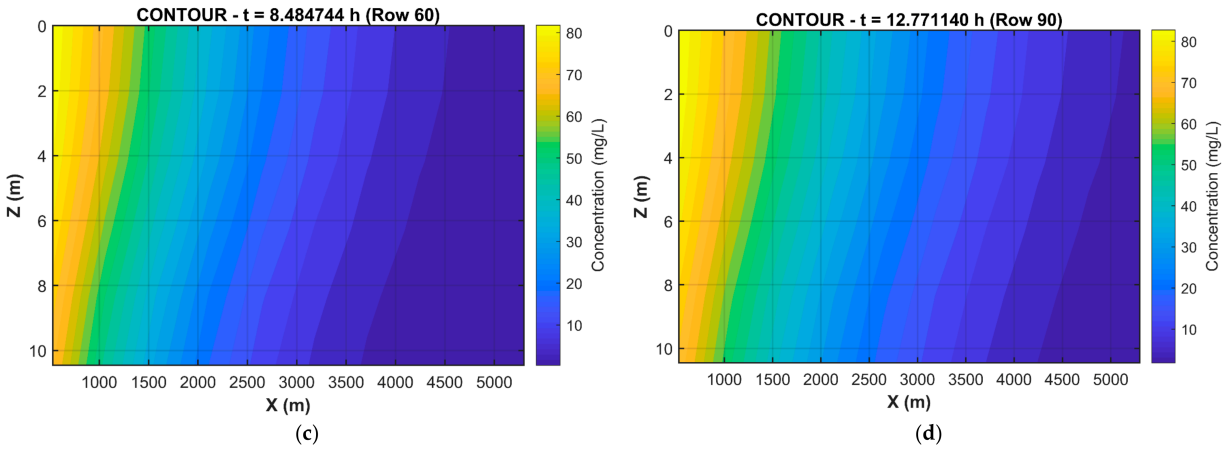


Figure 16. Contour and surface plots of longitudinal and vertical concentration profiles at y = 0 over a distance of 5300 m considering continuous input for (**a**) t = 0.72 h, (**b**) t = 4.24 h, (**c**) t = 8.48 h, and (**d**) t = 12.77 h.

3.5. Streeter–Phelps Model

From Equation (32), the fundamental Streeter–Phelps equations for carbonaceous biochemical oxygen demand (CBOD) and oxygen deficit are derived. These apply to water flows where only advective transport and the consumption rate of biochemical oxygen demand (BOD) are considered. Their solution under certain conditions was developed by Brenner [74]. These equations are applied under pseudo-steady conditions, meaning they are derived from the advection and reaction terms for both carbonaceous organic load and dissolved oxygen concentration, which is expressed in terms of the corresponding deficit.

$$V_x \frac{dL}{dx} = -k_d L. \tag{56}$$

By applying the change in variable $dx = V_x dt$, Equation (56) becomes:

$$\frac{dL}{dt} = -k_d L. \tag{57}$$

Equation (57) is the standard form of transport equation for carbonaceous biochemical oxygen demand. Similarly, the oxygen transport equation, considering advective transport and both deoxygenation and reaeration rates, is:

$$\frac{dC}{dt} = k_a(C_s - C) - k_d L. \tag{58}$$

Expressing Equation (58) in terms of oxygen deficit, defined as $D = C_S - C$, yields:

$$\frac{dD}{dt} = -k_a D + k_d L. \tag{59}$$

The differential contributions of deoxygenation and reaeration can also be expressed as:

$$\frac{dDeox}{dt} = -k_d L_0 exp(-k_d \times t), \tag{60}$$

$$\frac{dReox}{dt} = k_a(C_S - C). \tag{61}$$

A hybrid solution approach is proposed: analytical solutions are used to determine key parameters such as oxygen deficit, critical time, and critical distance, while numerical methods are applied for the full system resolution. The critical time is given by:

$$t_c = \left(\frac{1}{k_a - k_r}\right) \times ln\left[\frac{k_a}{k_r}\left(1 - \frac{D_0(k_a - k_r)}{k_d L_0}\right)\right]. \quad (62)$$

The critical deficit is:

$$D_c = \left(\frac{k_d \times L_0}{k_a}\right) \times \left[\frac{k_a}{k_r}\left(1 - \frac{D_0(k_a - k_r)}{k_d L_0}\right)\right]^{-\left(\frac{k_r}{k_a - k_r}\right)}. \quad (63)$$

The critical distance is:

$$x_c = \left(\frac{u}{k_a - k_r}\right) \times ln\left[\frac{k_a}{k_r}\left(1 - \frac{D_0(k_a - k_r)}{k_d L_0}\right)\right]. \quad (64)$$

Organic load depuration factor

The organic load purification factor in rivers and channels is a parameter that quantifies the natural capacity of a water body for self-purification, that is, its ability to reduce the biodegradable organic matter present. This process results from the combined action of mechanisms such as dilution, biological degradation, sedimentation, and water reoxygenation. In operational terms, the factor is defined as the fraction of organic load removed along a given reach of the river or channel, reflecting the efficiency of the physical, chemical, and biological processes involved in the recovery of water quality:

$$F_D = 1 - L/L_0 = 1 - exp(-k_d t) = 1 - exp(-k_d x/U). \quad (65)$$

Relationship between reaeration and deoxygenation constants

In hydrobiology and water quality studies, a self-purification index or global purification factor F_D^* is often defined as the ratio between the reoxygenation capacity k_a and the deoxygenation rate (k_d).

$$F_D^* = \frac{k_2}{k_1} = \frac{k_a}{k_r} = \frac{k_a}{k_d}. \quad (66)$$

This ratio provides an approximate measure of the self-purification capacity:

- If $F_D^* > 1$: High recovery capacity (reaeration dominates).
- If $F_D^* < 1$: Low recovery capacity (deoxygenation dominates).
- If $F_D^* \approx 1$: Unstable equilibrium.

Table 6 presents the equations and parameters used for the implementation of the developed computational model. For this purpose, the data reported in Table 5 were employed, complemented with additional information required for the proper implementation of the model. These parameters include the deoxygenation and reoxygenation constants adjusted as a function of temperature, salinity, and atmospheric pressure-variables that directly influence the process kinetics and the dynamics of dissolved oxygen. Additional empirical equations commonly used for estimating hydraulic variables and dispersion coefficients are summarized in Appendix A.

After processing the data in the corresponding computational program, the main results are reported, including a reduction in BOD from 100 ppm to 2.25 ppm; an oxygen deficit of 2.29; an organic load removal factor of 97.74%; a purification index of 1.9564; a critical time of 18.43 h; and a critical distance of 6.93 km. Additionally, Figure 17a shows the profile of the BOD decay rate, and Figure 17b presents the rate of change in the oxygen deficit corresponding to three different temperatures.

Table 6. Input data for the computational model.

Parameter	Equation/Data
Differential equations	(57)–(60)
Critical time	(62)
Critical deficit	(63)
Critical distance	(64)
Organic load removal factor	(65)
Self-purification index	(66)
Oxygen solubility (pure water vs. temperature)	(21)
Oxygen solubility (saline water)	(22)
Oxygen solubility (pressure-dependent)	(23)–(25)
Deoxygenation constant	1.44 day^{-1} (value obtained through model calibration Gray's Creek, Louisiana [68])
Reaeration constant	(26)
Deoxygenation and reoxygenation constants (temperature-dependent)	(29) and (30)
Flow rate	131 m^3 s^{-1}
Average width	120 m
Average depth	10.45
Atmospheric pressure	740 mmHg
Mean temperature of the mixed flow	10 °C
Salinity	5 g L^{-1} (assumed value)
Initial organic load	100 ppm (assumed value at the mixing point, considering the combined flow of the main stream and the tributary inflow)
Initial oxygen deficit	0.3 ppm (assumed value)
Simulation time	14.1 h

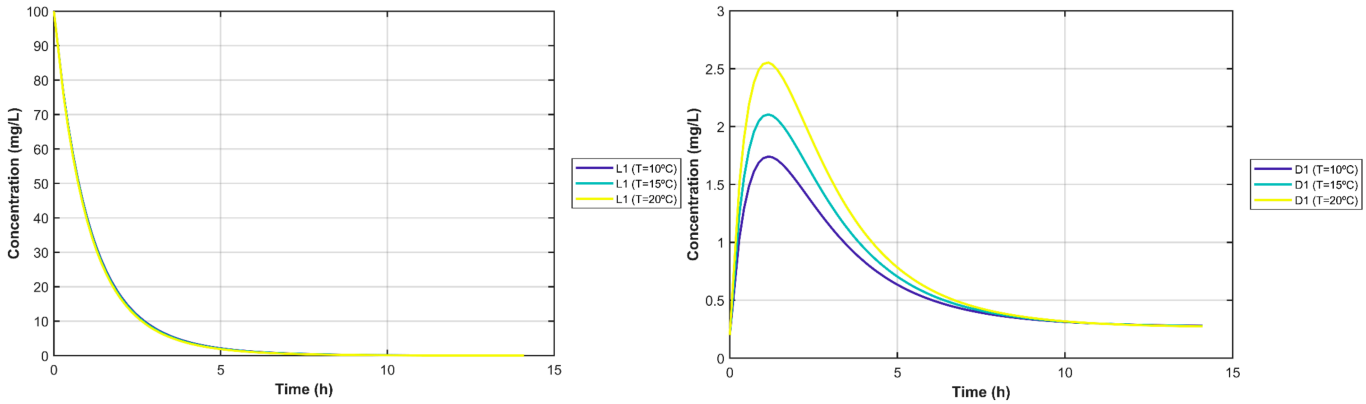


Figure 17. Modeling prediction of (**a**) Biochemical Oxygen Demand (BOD) profile by the Streeter–Phelps model, and (**b**) Oxygen deficit profile by the Streeter–Phelps model.

Although the Streeter–Phelps model is simpler to apply and interpret, it has limitations regarding the accuracy of its temporal and spatial predictions when compared with more sophisticated models such as the Advection–Dispersion–Reaction (ADR) model. The Streeter–Phelps model suggests that the complete recovery of a water body affected by organic pollution occurs after approximately 14.1 h. In contrast, the ADR model predicts recovery within only about 30 h, as it incorporates additional processes such as turbulent dispersion, which enhances oxygen distribution throughout the water column and accelerates the recovery process. This difference highlights the importance of physical mechanisms such as turbulence in promoting more efficient and rapid oxygen transport, thereby facili-

tating the restoration of river water quality. Therefore, while the Streeter–Phelps model remains valuable due to its simplicity and ease of implementation, its predictions may be less accurate than those obtained from more detailed models that explicitly account for turbulent transport processes.

3.6. Extended Streeter–Phelps Model with Advection, Diffusion, and Reaction (ADR) for Wastewater Purification

This is an extended version of the Streeter–Phelps model, in which unsteady-state and diffusive terms are incorporated. The analysis is carried out using a one-dimensional formulation, which adequately represents fast-flowing (turbulent) river systems and simplifies model implementation by neglecting transverse and vertical diffusion, thereby reducing the number of differential or algebraic equations required.

The conservation equations of the ADR model, corresponding to organic load and oxygen deficit, are given as follows:

$$\frac{\partial L}{\partial t} = -U\frac{\partial L}{\partial x} + D_T\frac{\partial^2 L}{\partial x^2} - k_r L, \tag{67}$$

$$\frac{\partial D}{\partial t} = -U\frac{\partial D}{\partial x} + D_T\frac{\partial^2 D}{\partial x^2} - k_a D + k_d L. \tag{68}$$

Equations (67) and (68) are initial value differential equations, whose solution is obtained using the Method of Lines. For this purpose, the right-hand side of the aforementioned equations is discretized, that is:

$$\frac{dL_i}{dt} = -U \times \frac{(L_i - L_{i-1})}{\Delta x} + D_T \times \frac{(L_{i+1} - 2L_i + L_{i-1})}{\Delta x^2} - k_r L_i, \tag{69}$$

$$\frac{dD_i}{dt} = -U \times \frac{(D_i - D_{i-1})}{\Delta x} + D_T \times \frac{(D_{i+1} - 2D_i + D_{i-1})}{\Delta x^2} - k_a D_i + k_d L_i. \tag{70}$$

With the initial conditions for the organic load:

$L_1(0) \neq 0$; $L_0(0) = 0$ (the upstream flow is free of biodegradable organic contaminants), $L_2(0) = 0$; $L_3(0) = 0$; …; $L_n(0) = 0$ (indicating that all other segments of the river section under study initially contain no organic load). This condition corresponds to a pulse-type input.

In the case of dissolved oxygen, at the initial time both upstream and downstream sections exhibit a defined deficit, that is: $D_i(0) = D_0 \; \forall i = 0 \ldots 10$.

Effectiveness Factor

By incorporating the longitudinal diffusion coefficient into the Streeter–Phelps model, it is possible to determine an effectiveness factor for both the organic load and the oxygen deficit through a time-dependent parameter.

For the organic load:

$$\eta_L = \frac{tanh(\phi_1)}{\phi_1}, \tag{71}$$

$$\phi_1 = \left[\frac{k_d L^2}{D_L t}\right]^{0.5}. \tag{72}$$

For the oxygen deficit:

$$\eta_D = \frac{k_a}{k_a + k_d}\frac{tanh(\phi_2)}{\phi_2}, \tag{73}$$

$$\phi_2 = \left[\frac{(k_a + k_d)L^2}{D_L t}\right]^{0.5}. \tag{74}$$

Figure 18a shows the biochemical oxygen demand (BOD) profile for the extended Streeter–Phelps model. It corresponds to a family of Gaussian-type curves with peaks that represent the concentration of organic matter at specific locations. The data used were obtained from Tables 5 and 6.

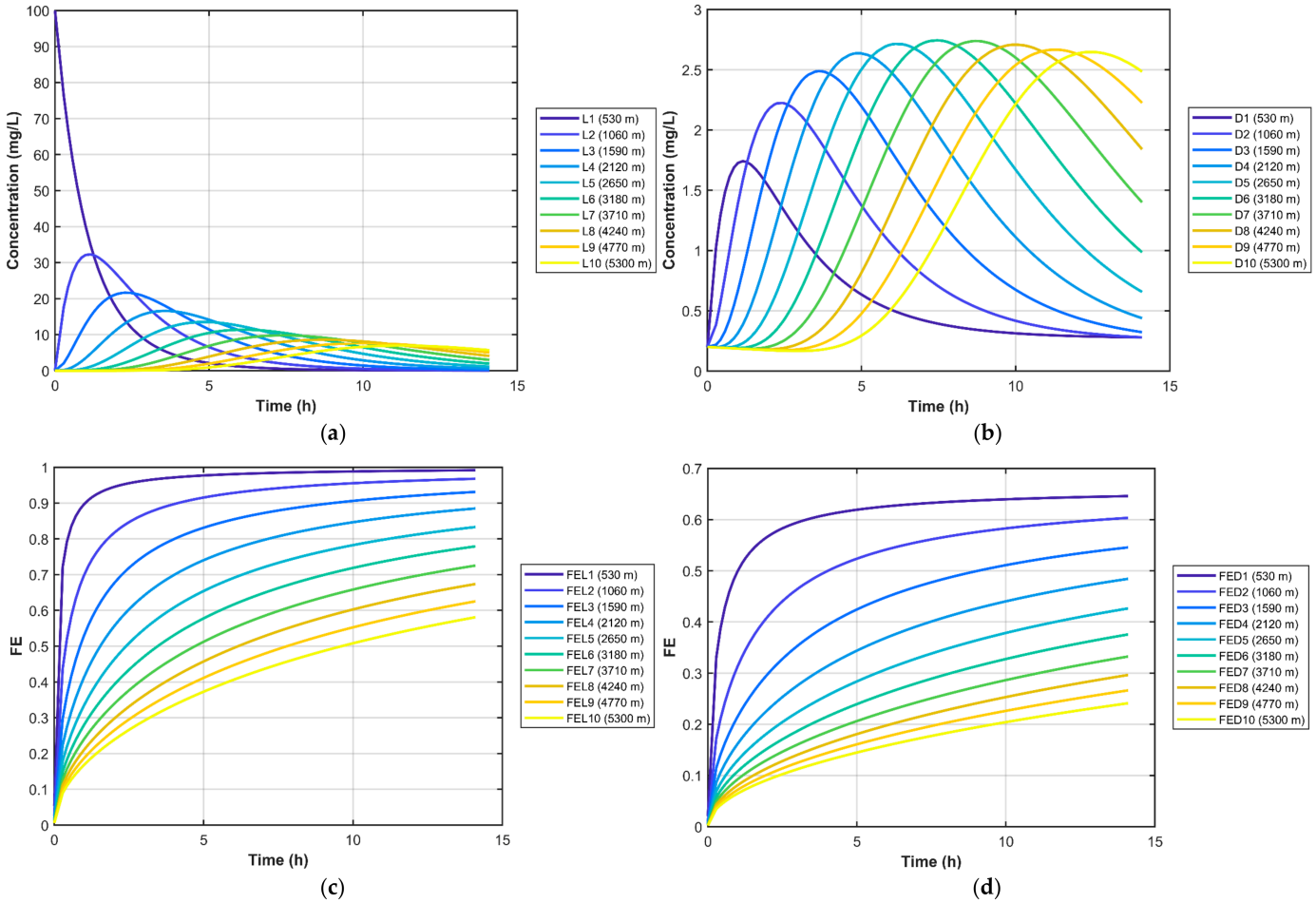


Figure 18. Temporal evolution of water quality indicators and effectiveness factors along the river system, (**a**) Organic matter degradation profile, (**b**) Oxygen deficit profile at each river segment as a function of time, (**c**) Transient effectiveness factor for biochemical oxygen demand, and (**d**) Transient effectiveness factor for oxygen deficit.

Figure 18b presents the oxygen deficit profile, which also exhibits pronounced peaks. However, after approximately 14.1 h (corresponding to the hydraulic residence time) the deficit begins to decrease. At around 30 h, it returns to its initial level prior to the organic loading event. This behavior indicates progressive recovery of dissolved oxygen levels following the pollution event.

Figure 18c,d show the transient (unsteady-state) effectiveness factor for the removal of organic load and for the oxygen deficit, respectively, as functions of time over a period of 14.1 h (hydraulic residence time).

4. Discussion

Regarding the diffusion coefficient

The statistical moments method constitutes an efficient tool for estimating the longitudinal dispersion coefficient from field tracer data. This approach provides a physically consistent prediction with reduced dependence on empirical parameters, while integrat-

ing flow anisotropy and attenuating experimental noise, thereby outperforming purely empirical or numerical methods [77].

The obtained value of the diffusion coefficient indicates effective longitudinal mixing, where velocity irregularities and turbulence enhance mass exchange. In practical terms, point concentration tends to homogenize within a few hours or over several kilometers downstream, depending on the mean flow velocity [78]. These results reinforce the validity of the ADR model, demonstrating that turbulent diffusion plays a key role in the natural self-purification of the system and in the recovery of dissolved oxygen following organic pollution events.

Regarding one-dimensional transport

The concentration–time curves exhibit Gaussian behavior, typical of processes dominated by turbulent dispersion and longitudinal mixing. Along 530 m segments, concentration peaks decrease with distance from the discharge point, reflecting the combined effects of dispersion, chemical degradation, and dilution. The contamination episode concludes at approximately 21 h, when the system reaches a quasi-steady state with minimal concentration variations.

The one-dimensional (1D) model adequately describes this behavior, as the flow is essentially linear, cross-sections are well mixed, and longitudinal dispersion dominates over lateral and vertical gradients. Under such conditions, the ADR equation provides a physically sound and computationally efficient representation [49].

Integration using Simpson's rule (1/3) up to 14.1 h (corresponding to the hydraulic residence time) based on Equation (42) shows that the effectiveness factor reaches 0.69 when only reaction is considered and 0.83 when diffusion is included, demonstrating that dispersion enhances system self-purification. Additionally, it is confirmed that the duration of the pollution pulse has a limited effect on this factor under constant mean velocity conditions.

In all cases, the Péclet number was found to be > 1, indicating that advection dominates over diffusion. Moreover, in the first eight segments of the river reach, transport dominates over reaction (Damköhler number Da < 1), whereas in the last two segments, reaction dominates (Da > 1).

Regarding the explicit one-dimensional transport method

The explicit finite difference method is a straightforward numerical approach for solving time-dependent partial differential equations, as it computes future values from previous data using recursive schemes. However, its computational implementation may become slow when fine grids or numerous time steps are required to ensure stability. Stability depends on dimensionless numbers such as the Péclet number (Pe), relating advective, and diffusive transport; the Courant–Friedrichs–Lewy number (C), linking flow progression with cell size; and the diffusive condition known as the Fourier number (Fo) [59], i.e., $P_{ex} = u\Delta x/D_L \leq 2$; $C = u\Delta t/\Delta x \leq 1$; $F_0 = D_L\Delta t/\Delta x^2 \leq 1/2$; $k\Delta t < 1$; $\Delta t \leq \frac{1}{k+u/\Delta x+2D_L/\Delta x^2}$.

Regarding the implicit method for one-dimensional transport

Although more complex than ODE-based approaches, this method allows the incorporation of sources, sinks, and spatiotemporal variations in concentration with greater detail. Unlike the explicit scheme, the implicit method applied to the ADR equation exhibits unconditional stability under linear conditions and constant coefficients, ensuring stable solutions even with large time steps. However, an appropriate relationship between time step and spatial grid must still be maintained to preserve resolution and minimize numerical diffusion, i.e., $F_o = D_L\Delta t/\Delta x^2 \leq 2$ [79].

Another highly stable method is the Crank–Nicolson scheme, a hybrid between explicit and implicit methods, where $F_o = D_L \Delta t / \Delta x^2 < 1$ (approximately ≤ 1) and $C = u\Delta t / \Delta x \leq 2$.

Regarding the two-dimensional model

Through adjustment or filtering of results, the two-dimensional model can reproduce patterns observed in the one-dimensional scheme, while also allowing the combination of different pollutant inputs (pulse or continuous discharges) that modify system dynamics until a quasi-steady state is reached.

Unlike the 1D model, the 2D approach provides a more realistic representation of advection, dispersion, and reaction processes in natural systems (rivers, lakes, or estuaries), as it accounts for both longitudinal and transverse variations. This improves spatial prediction of contaminants, optimizes control strategies, and serves as an intermediate step toward three-dimensional modeling, balancing accuracy and computational efficiency [49].

Regarding the three-dimensional model

The model generates a family of Gaussian-like curves downstream of the discharge, confirming the diffusive nature of the process. Under certain conditions, the three-dimensional model can be simplified to 2D or 1D formulations, reducing computational cost without losing representativeness.

It was observed that transverse and vertical diffusion coefficients are significantly lower than those reported for torrential streams, highlighting the need to recalibrate classical models for low-gradient rivers. The 3D approach provides a more realistic description of longitudinal, transverse, and vertical concentration variations, improving predictions of contaminant transport and supporting environmental control strategies [49,51].

Regarding the Streeter–Phelps model

The system exhibited a high self-purification index, indicating an effective response to organic matter input. However, around 18 h, a significant dissolved oxygen deficit was observed, attributed to intense biological consumption during decomposition. Subsequently, atmospheric and biological reaeration promoted gradual recovery, governed by the ratio between reaeration and deoxygenation constants (k_2/k_1 = 1.9).

Nevertheless, after 14.1 h of simulation, the oxygen concentration did not reach its initial level (10.28 ppm), stabilizing at 8.28 ppm, suggesting that full recovery requires more time due to slowly biodegradable organic compounds and limited oxygen transfer under stable hydraulic conditions [80,81].

An increase of 10 °C raised purification efficiency from 97% to 99% but reduced the self-purification rate to 1.5 due to lower dissolved oxygen solubility. This condition temporarily intensified the oxygen deficit and affected the balance between deoxygenation and reaeration. The final concentration was 8.07 ppm, indicating partial recovery influenced by thermal and hydraulic factors [82].

Regarding the modified Streeter–Phelps model

Figure 9 shows the dissolved oxygen deficit profile, where pronounced peaks are observed in early stages due to rapid oxygen consumption during oxidation of biodegradable organic matter. Around 14.1 h (corresponding to the hydraulic residence time) the deficit begins to decrease due to atmospheric reaeration and turbulent mixing. By approximately 30 h, the system recovers initial dissolved oxygen levels, indicating restoration of natural equilibrium after the contamination event.

This behavior is consistent with the Streeter–Phelps model, where the balance between deoxygenation (k_1) and reaeration (k_2) controls the magnitude and duration of the deficit, leading to a new steady state determined by hydraulic and biogeochemical conditions [80,82].

Regarding the effectiveness factor in the Streeter–Phelps model

At short distances, the Péclet number indicates that transport is governed jointly by advection and diffusion; however, beyond approximately 1000 m downstream, advection becomes dominant. Figure 15b,c shows that the effectiveness factor increases rapidly with time and tends to stabilize at longer times, while it decreases sharply with distance.

The initial 100 ppm pulse disperses rapidly, reaching very low concentrations at 5300 m, both at 14.1 h and 30 h. The BOD effectiveness factor remains high (0.73 at 30 h and 0.58 at 14.1 h), indicating that organic degradation occurs with minimal diffusion limitations. In contrast, the oxygen deficit effectiveness factor exhibits lower values (0.33 at 30 h and 0.24 at 14.1 h), highlighting that the balance between deoxygenation and reaeration limits dissolved oxygen recovery in the fluvial system [83].

5. Conclusions

In this study, the dispersion of soluble contaminants, both reactive and non-reactive, was analyzed using one-dimensional, two-dimensional, and three-dimensional transport frameworks, together with the evaluation of organic load and dissolved oxygen deficit based on the classical Streeter–Phelps model and its extended formulation incorporating diffusion terms for both variables. The results indicate that incorporating advective–diffusive mechanisms (ADR model) provides a more realistic representation of the spatial and temporal dynamics of contaminant transport in river systems.

The developed three-dimensional model, which accounts for velocity variations in the transverse and vertical directions, can be reformulated into an equivalent expression using a depth-average velocity dependent on the hydrodynamic conditions of the river. Furthermore, its mathematical structure allows consistent reduction to two-dimensional and one-dimensional formulations while preserving physical coherence, making it a flexible and scalable tool for comparative analysis across different levels of model complexity.

From a comparative perspective, the Streeter–Phelps model, although simpler and more straightforward to implement, exhibits limitations in capturing the spatial–temporal evolution of water quality processes. In contrast, the ADR model predicts significantly shorter recovery times, a difference mainly attributed to the inclusion of transverse turbulent diffusion, which enhances oxygen redistribution and accelerates system recovery.

From an applied standpoint, these findings highlight the importance of incorporating turbulent diffusion and hydrodynamic heterogeneity when assessing river self-purification capacity and designing water quality management strategies. Future work should focus on model validation using field data from different river systems and on extending the formulation to non-stationary flow conditions and variable hydrological regimes, in order to improve its applicability to more complex and realistic environmental scenarios.

The model employed in this study is based on idealizations commonly used in the water quality and transport phenomena literature, which allow for an analytical formulation but introduce limitations when applied to natural systems. In particular, constant density is assumed, implying that the effects of thermal stratification and variations caused by dissolved solids are neglected. This assumption is reasonable for freshwater rivers under moderately mixed conditions, but it may lead to deviations in systems characterized by significant thermal or salinity gradients [59,84]. In addition, the degradation of organic matter is represented by first-order kinetics, which constitutes an approximation that does not always capture the heterogeneity of natural or residual organic matter [85]. Finally, the channel geometry and flow are idealized as one-dimensional and steady-state, simplifying the analysis but not fully reproducing the hydraulic complexity of natural rivers. Taken together, these simplifications allow the model to be used as a first-approximation tool, and its results should therefore be interpreted within the context of these limitations.

The analysis was conducted under the assumptions of a regular channel geometry and constant flow rate, which simplifies the modeling process but limits the applicability of the results to real-world situations where these conditions may vary significantly. Furthermore, the study did not consider unsteady flow conditions or variations in river bathymetry, both of which can substantially influence contaminant dispersion and transport behavior. Future research should incorporate models that account for temporally varying flow conditions, as well as irregular bathymetry and spatially variable channel geometry, in order to achieve a more realistic representation of contaminant transport processes and improve the applicability of the results to complex and diverse natural riverine environments.

Author Contributions: Conceptualization, L.A.C.-V. and L.G.C.-P.; methodology, J.T.M.-C. and D.G.M.-H.; software, D.G.M.-H. and S.A.T.-P.; validation, C.G.-C. and R.P.-S.; formal analysis, H.R.C.-T.; investigation, L.G.C.-P. and H.R.C.-T.; resources, L.E.C.-G.; data curation, S.A.T.-P. and R.P.-S.; writing—original draft preparation, L.E.C.-G. and A.C.-V.; writing—review and editing, J.V.G.-F.; visualization, A.C.-V. and C.G.-C.; supervision, L.A.C.-V. and J.T.M.-C.; project administration, J.V.G.-F.; funding acquisition, L.A.C.-V. All authors have read and agreed to the published version of the manuscript.

Funding: This research was funded by the Faculty of Chemical Engineering at the National University of Callao.

Institutional Review Board Statement: Not applicable.

Informed Consent Statement: Not applicable.

Data Availability Statement: Data are contained within the article and/or can be requested via email.

Acknowledgments: The authors acknowledge the administrative and support staff of the Faculty of Chemical Engineering at the National University of Callao.

Conflicts of Interest: The authors declare no conflicts of interest.

Appendix A

Equations for Model Parameter Estimation.

Flow Velocity and Discharge

In the literature, various empirical equations are shown for calculating discharge; one of these equations is the Chezy formula, used to calculate velocity and discharge in straight channels without backwater effects or flow divergence or convergence [86].

The velocity is obtained by:

$$V = C\sqrt{R \times S}$$

V: Mean flow velocity (m s^{-1});
C: Chezy coefficient (dimensionless, depends on roughness and channel conditions);
R: Hydraulic mean radius (m); A/P with A: flow area (m^2); P: wetted perimeter (m);
S: Hydraulic slope of the channel (approximately the bed slope, dimensionless).
The discharge is obtained by:

$$Q = A \times V = A \times C\sqrt{R \times S}$$

Q: Volumetric flow or discharge (m^3 s^{-1}).

Another equation for calculating velocity and discharge is Manning's equation, which predicts flow resistance in meandering channels considering geometric and hydraulic parameters, Reynolds and Froude numbers, and bed slope and sinuosity [87].

Velocity and discharge, respectively, are calculated by:

$$V = \frac{1}{n} R^{2/3} S^{1/2}$$

$$Q = \frac{1}{n} A \times R^{2/3} S^{1/2}$$

V: Fluid velocity (m s^{-1});
A: Flow area (m^2);
R: Hydraulic mean radius (m); A/P with A: flow area (m^2); P: wetted perimeter (m);
S: Hydraulic slope of the channel (dimensionless);
n: Manning roughness coefficient (s $m^{-1/3}$), which depends on the characteristics of the channel surface.

Another simple and practical alternative to obtaining the mean velocity in a river through field measurements is the float method, in which the surface velocity is measured with a floating object and adjusted with an empirical coefficient [88]:

$$V_m = 0.85 \times V_{sup}$$

V_{sup}: Mean velocity at the river surface.

An important equation to obtaining the maximum surface velocity in laminar regime in rivers and channels is given by:

$$V_{max} = k \times V$$

V: Mean flow velocity in the channel or river (m s^{-1});
V_{max}: Maximum flow velocity in the channel or river (m s^{-1}).

With k between 1.15 and 1.25 according to the W/H ratio (empirical correction coefficient); and for turbulent regime, the Nikuradse equation is used, given by:

$$V(z) = \frac{U^*}{k} ln(\frac{z}{k_s}) + B$$

U^*: Shear velocity (m s^{-1}).
k: Von Karman constant ≈ 0.41.
k_s : Absolute or Nikuradse roughness. Typical value for a natural channel = 0.003 m.
B: Empirical constant for a rough medium ≈ 8.5.
At the surface $z = H$, the maximum velocity is obtained by:

$$V_{max} = \frac{U^*}{k} \ln(\frac{z}{k_s}) + BU^*$$

$$U^* = V\sqrt{f/8}$$

V: Mean velocity (m s^{-1});
f: Darcy–Weisbach friction factor.
For rough channels, Nikuradse proposes the calculation of the friction factor by:

$$\frac{1}{\sqrt{f}} = -2log_{10}\left(\frac{k_s}{14.H}\right)$$

H: Mean fluid depth (m).

Longitudinal Dispersion Coefficient

Fischer equation [49]: The longitudinal dispersion coefficient is fundamental for modeling the transport of contaminants in lotic water bodies. For its estimation, various empirical and analytical formulations have been developed. Among them, the Fischer equation stands out, which uses a double integral based on the transverse and vertical velocity distribution to determine this coefficient in channels and rivers [51,89].

$$D_L = \frac{1}{UA^2} \iint_A \tau \Big(V_x(y,z) - U \Big)^2 dA$$

D_L: Longitudinal dispersion coefficient (m s^{-1});
A: Cross-sectional area of the channel or river (m^2);
U: Mean velocity in the longitudinal direction (m s^{-1});
$V_x(y,z)$: Local velocity in the longitudinal direction (m s^{-1});
dA: Differential area element in the cross section (m^2);
τ: Lateral and vertical mixing time scale (controlled by transverse and vertical diffusion).
Before equation is equivalent to:

$$D_L = \frac{1}{UA^2} \iiint_v \Big(V_x(y,z) - U \Big)^2 dv$$

The integral in Equation (21) represents the contribution of the fluctuations of the local velocity with respect to the mean velocity. These fluctuations generate additional solute transport (dispersion) when interacting with lateral and vertical diffusion processes. Fischer demonstrated that:

$$\tau \sim \frac{W^2}{E_y} \; y \;\; \tau \sim \frac{H^2}{E_z}$$

W: Half-width of the channel or river (m);
H: Depth of the channel or river (m);
E_y: Transverse dispersion coefficient (m^2 s^{-1});
E_z: Vertical dispersion coefficient (m^2 s^{-1}).
For rivers and channels, Fischer simplified the integral into an empirical expression that is frequently used in field applications:

$$D_L \approx 0.011 \frac{U^2 W H}{E_y + E_z}$$

D_L: Longitudinal diffusion coefficient (m^2 s^{-1}).
Deng et al. equation [47]: It simplifies Fischer's triple integral and adapts it to the geometric characteristics of the channel [90]. It derived a theoretical expression to calculate D_L based on the shape of the transverse depth profile, the distribution of local velocities, and the integration of Fischer's triple integral, improved by an updated transverse mixing coefficient; one of the final empirical forms proposed is the following:

$$D_L = \alpha U B H \left(\frac{U}{U^*} \right)$$

D_L: Longitudinal dispersion coefficient (m^2 s^{-1});
U: Mean longitudinal velocity (m s^{-1}):
B: Effective channel width (m);
H: Mean depth (m);
U^*: Shear velocity (m s^{-1});
α: Empirical constant derived from fitting with field data.

Sahay and Dutta equation [91]: It considers channel sinuosity, improving accuracy in sinuous rivers [91,92]; the corresponding equation is:

$$\frac{D_L}{UH} = a\left(\frac{B}{H}\right)^b\left(\frac{U}{U^*}\right)^c$$

D_L: Longitudinal dispersion coefficient ($m^2\ s^{-1}$);
U: Mean longitudinal velocity ($m\ s^{-1}$);
B: Effective channel width (m);
H: Mean depth (m);
U^*: Mean Depth ($m\ s^{-1}$), defined as $U^* = \sqrt{\tau_0/\rho}$; τ_0: shear stress at the bed ($N\ m^{-2}$) and ρ the water density ($kg\ m^{-3}$);
$a, b\ y\ c$: Empirical coefficients determined by fitting with genetic algorithms from field-measured data of the relationships given in Equation (25).

Many of the dispersion coefficients are expressed in terms of mean velocity, shear velocity, channel width, and depth in $m^2\ s^{-1}$ [93]; some of the reported values are:

McQuivey and Keefer [94]:

$$D_L = 0.058 \times \frac{Q}{SB}\ F \leq 0.5$$

Fischer [45]:

$$D_L = 0.011 \times \frac{U^2B^2}{HU^*}$$

Seo and Cheong [95]:

$$D_L = 5.915 \times HU^*\left(\frac{B}{H}\right)^{0.620}\left(\frac{U}{U^*}\right)^{1.428}$$

Koussis and Rodríguez-Mirasol [96]:

$$D_L = 0.6 \times \frac{U^*B^2}{H}$$

Kashefipour and Falconer [97]:

$$D_L = 10.612 \times HU\left(\frac{U}{U^*}\right)$$

Kashefipour and Falconer [97]:

$$D_L = \left[7.428 + 1.775\left(\frac{B}{H}\right)^{0.620}\left(\frac{U^*}{U}\right)^{0.572}\right]HU\left(\frac{U}{U^*}\right)$$

The units of the dispersion coefficient are as follows:
D_L: Longitudinal dispersion coefficient ($m^2\ s^{-1}$);
B: Channel width (m);
U: Mean flow velocity ($m\ s^{-1}$);
U^*: Shear velocity ($m\ s^{-1}$);
H: Flow depth (m);
Q: Volumetric flow rate ($m^3\ s^{-1}$);
S: Channel slope.

Longitudinal Dispersion Coefficient

Seo and Cheong's regression formula [46]:

$$\frac{D_T}{U^* H} = 5.915 \times \left(\frac{B}{H}\right)^{-0.878}$$

Deng et al.'s formula [47]:

$$D_T = \beta U^* H \left(\frac{B}{H}\right)^n$$

where β and n are empirical fitting parameters ($\beta \approx 0.145$, $n = 0.62$).

Jeon et al.'s equation: The normalized transverse dispersion coefficient is related to several hydraulic and geometric parameters [98], through:

$$\frac{D_T}{U^* H} = 0.029 \times \left(\frac{U}{U^*}\right)^{0.463} \left(\frac{W}{H}\right)^{0.299} S_n^{0.733}$$

The units of the above equations are the same as those indicated for the longitudinal dispersion coefficient; that is:

D_T: Transverse diffusion coefficient ($m^2\ s^{-1}$);

U: Mean longitudinal flow velocity, ($m\ s^{-1}$);

S_n: Channel sinuosity, defined as the ratio between the actual channel length following all its curves and the straight-line length (dimensionless); the remaining terms retain the same nomenclature;

$U^* = \sqrt{\tau_0/\rho}$: Shear velocity ($m\ s^{-1}$);

τ_0: Shear stress at the bed ($N\ m^{-2}$);

H: Hydraulic depth (m);

B: Channel width (m).

Vertical Dispersion Coefficient

Fischer formula, based on field measurements:

$$D_V = \beta \times U^* H,$$

with β in the range $0.05 \leq \beta \leq 0.1$.

Seo and Cheong formula:

$$D_V = \beta \times U^* D_V = \gamma \times U^* H$$

with $\gamma \approx 0.079$.

Kinetic Constant

Ammonium from fertilizer, in the absence of bacteria, is chemically oxidized by oxygen; in the presence of bacteria such as *Nitrobacter vulgaris*, *Nitrobacter hamburgensis*, *Nitrobacter winogradskyi*, *Nitrospira moscoviensis*, etc., it degrades following the Michaelis–Menten mechanism. In the case of *Nitrobacter vulgaris*, ammonium oxidation to nitrite has values of $K_M = 49 \pm 11$ μM NO_2^- and $V_{max} = 164 \pm 9$ μM NO_2^-/mg protein h^{-1}; this and other data for constants related to other bacteria are reported in [99]; the effects of temperature changes on oxidation rate are shown by [100].

In natural waters of rivers and lakes, Ryzhakov et al. determined first-order constants for nitrification in the range of 0.01–0.1 day^{-1}, consistent with values obtained by other methods [101]; in surface waters of the U.S., the kinetic constant varies between 0.02 y 0.09 day^{-1}; laboratory values for ammonium nitrification with bacteria such as *Nitrosomonas* typically fall within k ≈ 0.05 a 0.2 day^{-1} at standard temperatures [102].

Reaeration Constant

Long: Proposes the relationship known as the Texas equation, based on data collected on streams in Texas [103]:

$$k_a = 1.923 \times \frac{U^{0.273}}{H^{0.984}}$$

Isaacs and Gaudy: Equation developed using regression analysis of data collected in a recirculating channel in a cylindrical tank; later correlated with Churchill's field data, obtaining new coefficients [104]:

$$k_a = 4.75 \times \frac{U}{H^{1.5}}$$

Cadwallader and McDonnell: Based on multivariate analysis of reaeration data from Churchill and Owens [105]:

$$k_a = 185.5 \times \frac{U \times S^{0.5}}{H}$$

$$0.06 \leq H \leq 0.274; 0.0305 \leq U \leq 0.213;\ 0.00004 \leq S \leq 0.00092; 0.26 \leq k_a \leq 8.5$$

Padden and Gloyna: Through regression and analysis of experimental data [106]:

$$k_a = 4.547 \times \frac{U^{0.703}}{H^{1.054}}$$

where

k_a: k_2 in (day^{-1});
U: Flow velocity (m s^{-1});
H: Flow depth (m);
S: Channel slope.

References

1. Oznobikhina, L.A. Pollution of Ecosystem Water Resources in the Ural Federal District. *IOP Conf. Ser. Earth Environ. Sci.* **2022**, *1045*, 012125. [CrossRef]
2. Dwivedi, S.; Shikha, D. Water Pollution: Causes, Effects and Control. *Biochem. Cell Arch.* **2016**, *16*, 96–102.
3. Sudhakar, M.S.; Kumar, S.S. Toxicity of Surface Water Bodies and Public Health. In *Toxicity of Aquatic System and Remediation: The Contemporary Issues*; CRC Press: Boca Raton, FL, USA, 2024; pp. 70–84.
4. Naqvi, H.R.; Mutreja, G.; Hashim, M.; Singh, A.; Nawazuzzoha, M.; Naqvi, D.F.; Siddiqui, M.A.; Shakeel, A.; Chaudhary, A.A.; Naqvi, A.R. Global Assessment of Tropospheric and Ground Air Pollutants and Its Correlation with COVID-19. *Atmos. Pollut. Res.* **2021**, *12*, 101172. [CrossRef] [PubMed]
5. Siddiqui, M.H.; Bhanbhro, U.; Shaikh, K.; Ahmed, S.; Begum, R.; Shoukat, S.; Khokhar, W.A. Seasonal Occurrence and Ecological Risk Assessment of Polycyclic Aromatic Hydrocarbons in the Sediments and Water in the Left-Bank Canals of Indus River, Pakistan. *Environ. Monit. Assess.* **2024**, *196*, 1165. [CrossRef] [PubMed]
6. Taylor, S.D.; He, Y.; Hiscock, K.M. Modelling the Impacts of Agricultural Management Practices on River Water Quality in Eastern England. *J. Environ. Manag.* **2016**, *180*, 147–163. [CrossRef] [PubMed]
7. Soukhri, D.N.M.; Faudzi, S.M.M.; Yusof, Z.; Akhir, M.F.M.; Kamal, N.M.; Saad, N.A. A Review on Factors to Be Incorporated in Water Quality Study. *J. Kejuruter.* **2022**, *34*, 575–583. [CrossRef] [PubMed]
8. Kottaiveeran, K. An Economic Analysis of Drinking Water Pollution In Tiruppur. *Pollut. Res.* **2011**, *30*, 495–499.
9. Withanachchi, S.S.; Ghambashidze, G.; Kunchulia, I.; Urushadze, T.; Ploeger, A. Water Quality in Surface Water: A Preliminary Assessment of Heavy Metal Contamination of the Mashavera River, Georgia. *Int. J. Environ. Res. Public Health* **2018**, *15*, 621. [CrossRef] [PubMed]
10. Reddy, K.R.C.; Singh, P. Different Modes of Water Pollution. *Indian J. Environ. Prot.* **2008**, *28*, 420–421.
11. Nithya, R.; Vinodhini, P.A.; Vinoth, J. Biocomposites and Polymer Blends for Wastewater Treatment. In *Industrial Applications of Marine Biopolymers*; Sudha, P.N., Ed.; CRC Press: Boca Raton, FL, USA, 2017; pp. 473–499.
12. Pasha, A.B.M.K.; Nur, M.S.; Mozumder, S.; Parveen, M. Impact of River Water Quality on Public Health in Perspective of Asian Rivers: A Case Study of Buriganga River, Bangladesh. *J. Environ. Earth Sci.* **2023**, *5*, 1–16. [CrossRef]

13. de Almeida Araújo, Y.; de Almeida Ferreira, E.; Fernandes, R.; Henry-Silva, G.G.; de Oliveira, F.É.R.; Tavares, V.N.S.; Portela, J.C.; da Cunha, M.L.; da Costa Chagas, N.R.; de Sousa Antunes, L.F.; et al. Assessment of Water and Sediment Quality in Intermittent Streams across Different Land Uses in the Brazilian Semiarid Region: Implications for Sustainable Irrigation and Resource Management. *Environ. Sci. Pollut. Res.* **2025**, *32*, 8873–8892. [CrossRef] [PubMed]
14. Flores-Valenzuela, L.E.; González-Fernández, J.V.; Carranza-Oropeza, M.V. Hydrogel Applicability for the Industrial Effluent Treatment: A Systematic Review and Bibliometric Analysis. *Polymers* **2023**, *15*, 2417. [CrossRef] [PubMed]
15. Ismail, H.; Syed Hussain, T.P.R.; Subhan, M. The Impact of Spatial Development on Water Pollution: A Comparative Assessment of River Water Quality in Two Municipalities in Malaysia. *Int. J. Environ. Sustain. Dev.* **2020**, *19*, 333–342. [CrossRef]
16. Ramadan, E.M.; Fahmy, M.R.; Nosair, A.M.M.; Badr, A.M. Using Geographic Information System (GIS) Modeling in Evaluation of Canals Water Quality in Sharkia Governorate, East Nile Delta, Egypt. *Model. Earth Syst. Environ.* **2019**, *5*, 1925–1939. [CrossRef]
17. Rashid, M.K.; Salman, I.R.; Obaid, A.L.; Hassan, S.A.D.H.; Al-Musawi, M.R.; Al-Saady, M. Application of Machine Learning in Predicting Sources of Water Pollution in the Euphrates and Tigris Rivers in Iraq. *Int. J. Aquat. Biol.* **2024**, *12*, 581–589. [CrossRef]
18. Neamtu, R.; Sluser, B.; Plavan, O.; Teodosiu, C. Environmental Monitoring and Impact Assessment of Prut River Cross-Border Pollution. *Environ. Monit. Assess.* **2021**, *193*, 340. [CrossRef] [PubMed]
19. Bessa Santos, R.M.; Farias do Valle Junior, R.; Abreu Pires de Melo Silva, M.M.; Tarlé Pissarra, T.C.; Carvalho de Melo, M.; Valera, C.A.; Leal Pacheco, F.A.; Sanches Fernandes, L.F. A Framework Model to Integrate Sources and Pathways in the Assessment of River Water Pollution. *Environ. Pollut.* **2024**, *347*, 123661. [CrossRef] [PubMed]
20. Yuceer, M.; Coskun, M.A. Modeling Water Quality in Rivers: A Case Study of Beylerderesi River in Turkey. *Appl. Ecol. Environ. Res.* **2016**, *14*, 383–395. [CrossRef]
21. Amin, A.Z.M.; Amin, A.F.M.; Gani, U.K.A. Mathematical Modelling in the River Pollution: One Dimensional Advection Diffusion of River Pollution in Semi Infinite Media Inverse Laplace Transforms. *AIP Conf. Proc.* **2023**, *2582*, 020007. [CrossRef]
22. Wan, L.; Wang, H. Control of Urban River Water Pollution Is Studied Based on SMS. *Environ. Technol. Innov.* **2021**, *22*, 101468. [CrossRef]
23. Zhu, L.; Chen, Y.; Wang, Y.; Wei, Y.; Zheng, H.; Zhang, Y. A Comprehensive Analysis of Impacts of Socio-Economic Development and Land Use on River Water Quality in a Megacity-Region: A Case Study. *Environ. Res. Commun.* **2023**, *5*, 025006. [CrossRef]
24. Ren, X.; Yang, C.; Zhao, B.; Xiao, J.; Gao, D.; Zhang, H. Water Quality Assessment and Pollution Source Apportionment Using Multivariate Statistical and PMF Receptor Modeling Techniques in a Sub-Watershed of the Upper Yangtze River, Southwest China. *Environ. Geochem. Health* **2023**, *45*, 6869–6887. [CrossRef] [PubMed]
25. Omarova, P.; Amirgaliyev, Y.; Kozbakova, A.; Ataniyazova, A. Application of Physics-Informed Neural Networks to River Silting Simulation. *Appl. Sci.* **2023**, *13*, 11983. [CrossRef]
26. Romanowicz, R.J. Application of Optimal Nonstationary Time Series Analysis to Water Quality Data and Pollutant Transport Modelling. In *System Identification, Environmental Modelling, and Control System Design*; Wang, L., Garnier, H., Eds.; Springer: London, UK, 2012; pp. 501–518.
27. Duarte, A.A.L.S.; Boaventura, R.A.R. Pollutant Dispersion Modelling for Portuguese River Water Uses Protection Linked to Tracer Dye Experimental Data. *WSEAS Trans. Environ. Dev.* **2008**, *4*, 1047–1056.
28. de Barros, F.P.J.; Mills, W.B.; Cotta, R.M. Integral Transform Solution of a Two-Dimensional Model for Contaminant Dispersion in Rivers and Channels with Spatially Variable Coefficients. *Environ. Model. Softw.* **2006**, *21*, 699–709. [CrossRef]
29. Machado, M.B.; Furlan, L.T.; Tomaz, E.; Nunhez, J.R. Modeling Multiple Emissions in a River. In *Proceedings of the AIChE Annual Meeting Conference Proceedings*; American Institute of Chemical Engineers: New York, NY, USA, 2005.
30. Machado, M.B.; Furlan, L.T.; Tomaz, E.; Nunhez, J.R. A 3-D Model for Oxygen Consumption in a River Using Computational Fluid Dynamics (CFD). In *Proceedings of the AIChE Annual Meeting, Conference Proceedings*; American Institute of Chemical Engineers: New York, NY, USA, 2004; pp. 7045–7054.
31. Zhang, H.; Yang, Y.; Li, S.; Kang, S. Research on Chemical Leakage Based on Three-Dimensional Soluble Contaminant Diffusion Model. *Rev. Chim.* **2020**, *71*, 523–535. [CrossRef]
32. Zhang, J.W.; Wu, W.Q. Numerical Simulation Study of Soluble and Conservative Liquid Chemicals Diffusion in Tidal River. *Adv. Mat. Res.* **2014**, *864–867*, 1427–1432. [CrossRef]
33. Milišić, H.; Hadžić, E.; Jusić, S. Estimation of Longitudinal Dispersion Coefficient Using Field Experimental Data and 1D Numerical Model of Solute Transport. *Lect. Notes Netw. Syst.* **2020**, *83*, 305–323. [CrossRef]
34. Olowe, K.O.; Kumarasamy, M. Development of the Hybrid Cells in Series Model to Simulate Ammonia Nutrient Pollutant Transport along the Umgeni River. *Environ. Sci. Pollut. Res.* **2017**, *24*, 22967–22979. [CrossRef] [PubMed]
35. Park, I.; Seo, I.W.; Do Kim, Y.; Song, C.G. Flow and Dispersion Analysis of Shallow Water Problems with Froude Number Variation. *Environ. Earth Sci.* **2016**, *75*, 120. [CrossRef]
36. Khaldi, N.; Chouari, Y.; Mhiri, H.; Bournot, P. Pulsation Effects on Pollutant and Sediment Transport in Free-Surface Flow. *Environ. Pollut.* **2016**, *219*, 685–695. [CrossRef] [PubMed]

37. Park, I.; Seo, I.W.; Shin, J.; Song, C.G. Experimental and Numerical Investigations of Spatially-Varying Dispersion Tensors Based on Vertical Velocity Profile and Depth-Averaged Flow Field. *Adv. Water Resour.* **2020**, *142*, 103606. [CrossRef]
38. Zima, P.; Sawicki, J. Numerical Analysis of the Influence of 2D Dispersion Parameters on the Spread of Pollutants in the Coastal Zone. *Water* **2024**, *16*, 3637. [CrossRef]
39. White, F.M. *Fluid Mechanics*, 7th ed.; McGraw-Hill: Columbus, OH, USA, 2011.
40. Shah, R.K.; London, A.L. *Laminar Flow Forced Convection in Ducts*; Academic Press: New York, NY, USA, 1978.
41. Karami Cheme, E.; Mazaheri, M. The Effect of Neglecting Spatial Variations of the Parameters in Pollutant Transport Modeling in Rivers. *Environ. Fluid Mech.* **2021**, *21*, 587–603. [CrossRef]
42. Seo, I.W.; Shin, J.; Bang, J.Y. Dispersion Coefficients of Contaminant Transport Model for River Mixing Analysis. In *Proceedings of the IAHR World Congress*; Seo, I.W., Shin, J., Bang, J.Y., Eds.; International Association for Hydro-Environment Engineering and Research: Madrid, Spain, 2019; pp. 654–659.
43. Ginzburg, I.; Vikhansky, A. Determination of the Diffusivity, Dispersion, Skewness and Kurtosis in Heterogeneous Porous Flow. Part I: Analytical Solutions with the Extended Method of Moments. *Adv. Water Resour.* **2018**, *115*, 60–87. [CrossRef]
44. Potter, M.; Wiggert, D. *Mecánica de Fluidos*, 3rd ed.; Thomson: Mexico City, Mexico, 2002.
45. Fischer, H.B. Discussion of "Simple Method for Predicting Dispersion in Streams". *J. Environ. Eng. Div.* **1975**, *101*, 453–455. [CrossRef]
46. Baek, K.O.; Seo, I.I.W. Modifying Elder's Longitudinal Dispersion Coefficient for Two-Dimensional Solute Mixing Analysis in Open-Channel Bends. *Water* **2022**, *14*, 2962. [CrossRef]
47. Baek, K.O.; Seo, I.W. Estimation of the Transverse Dispersion Coefficient for Two-Dimensional Models of Mixing in Natural Streams. *J. Hydro-Environ. Res.* **2017**, *15*, 67–74. [CrossRef]
48. Kang, S.; Park, S.M.; Park, J.G.; Baek, K. Enhanced Adsorption of Arsenic Using Calcined Alginate Bead Containing Alum Sludge from Water Treatment Facilities. *J. Environ. Manag.* **2019**, *234*, 181–188. [CrossRef] [PubMed]
49. Fischer, H.B.; List, E.J.; Koh, R.C.Y.; Imberger, J.; Brooks, N.H. *Mixing in Inland and Coastal Waters*; Academic Press: New York, NY, USA, 1979.
50. Baek, K.O. Flowchart on Choosing Optimal Method of Observing Transverse Dispersion Coefficient for Solute Transport in Open Channel Flow. *Sustainability* **2018**, *10*, 1332. [CrossRef]
51. Chen, Y.; Wang, Z.; Zhu, D.; Liu, Z. Longitudinal Dispersion Coefficient in Ice-Covered Rivers. *J. Hydraul. Res.* **2016**, *54*, 558–566. [CrossRef]
52. Schwab, L.E.; Rehmann, C.R. Importance of Vertical Variations of Velocity for Shear Dispersion in Rivers. *J. Hydraul. Eng.* **2015**, *141*, 06015011. [CrossRef]
53. Legleiter, C.J.; Manley, P.V.; Erwin, S.O.; Bulliner, E.A. An Experimental Evaluation of the Feasibility of Inferring Concentrations of a Visible Tracer Dye from Remotely Sensed Data in Turbid Rivers. *Remote Sens.* **2020**, *12*, 57. [CrossRef]
54. Xuetong, G.; Yun, W. Study on Connectivity of Karst Water Conduction Channel in the Process of Pit Water Sealing. *China Min. Mag.* **2021**, *30*, 173–177. [CrossRef]
55. Kim, K.C.; Park, G.H.; Jung, S.H.; Lee, J.L.; Suh, K.S. Analysis on the Characteristics of a Pollutant Dispersion in River Environment. *Ann. Nucl. Energy* **2011**, *38*, 232–237. [CrossRef]
56. Millero, F.J.; Huang, F. Solubility of Oxygen in Aqueous Solutions of KCl, K_2SO_4, and $CaCl_2$ as a Function of Concentration and Temperature. *J. Chem. Eng. Data* **2003**, *48*, 1050–1054. [CrossRef]
57. Valderrama, J.O.; Campusano, R.A.; Forero, L.A. A New Generalized Henry-Setschenow Equation for Predicting the Solubility of Air Gases (Oxygen, Nitrogen and Argon) in Seawater and Saline Solutions. *J. Mol. Liq.* **2016**, *222*, 1218–1227. [CrossRef]
58. Debelius, B.; Gómez-Parra, A.; Forja, J.M. Oxygen Solubility in Evaporated Seawater as a Function of Temperature and Salinity. *Hydrobiologia* **2009**, *632*, 157–165. [CrossRef]
59. Chapra, S.C.; Pelletier, G.J.; Tao, H. *A Modeling Framework for Simulating River and Stream Water Quality. Documentation and User's Manual*; Civil and Environmental Engineering Department, Tufts University: Medford, MA, USA, 2008.
60. Ji, Z.G. *Hydrodynamics and Water Quality: Modeling Rivers, Lakes and Estuaries*; John Wiley and Sons, Inc.: Hoboken, NJ, USA, 2008.
61. Bowie, G.L.; Mills, W.B.; Porcella, D.B.; Campbell, C.L.; Pagenkopf, J.R.; Rupp, G.L.; Johnson, K.M.; Chan, P.W.H.; Gherini, S.A. *Rates, Constants, and Kinetics Formulations in Surface Water Quality Modeling*, 2nd ed.; Barnwell, T.O., Ed.; United States Environmental Protection Agency: Athens, GA, USA, 1985.
62. Le, T.T.H.; Fettig, J.; Meon, G. Kinetics and Simulation of Nitrification at Various PH Values of a Polluted River in the Tropics. *Ecohydrol. Hydrobiol.* **2019**, *19*, 54–65. [CrossRef]
63. Cleave, M. Water Quality Relationships to Flow—Streams and Estuaries. In *Methodologies for the Determination of Stream Resource Flow Requirements: An Assessment*; Stalnaker, C.B., Arnette, J.L., Eds.; US Fish and Wildlife Service Office of Biological Services Western Water Allocation: Logan, UT, USA, 1976; pp. 35–88.
64. Bansal, M.K. Deoxygenation in Natural Streams. *JAWRA J. Am. Water Resour. Assoc.* **1975**, *11*, 491–504. [CrossRef]

65. Novotny, V.; Krenkel, P.A. A Waste Assimilative Capacity Model for a Shallow, Turbulent Stream. *Water Res.* **1975**, *9*, 233–241. [CrossRef]
66. Miller, J.E.; Jennings, M.E. Modeling Nitrogen, Oxygen, Chattahoochee River, Ga. *J. Environ. Eng. Div.* **1979**, *105*, 641–653. [CrossRef]
67. Grenney, W.J.; Kraszewski, A.K. *Description and Application of the Stream Simulation and Assessment Model: Version IV (SSAM IV)*; United States Department of the Interior: Fort Collins, CO, USA, 1981.
68. Crane, S.M. *Reliability Analysis of BOD Kinetics in a Small, Southern Stream Governed by the Discharge of an Oxidation Pond*; Louisiana State University: Baton Rouge, LA, USA, 1981.
69. Hvitved-Jacobsen, T. The Impact of Combined Sewer Overflows on the Dissolved Oxygen Concentration of a River. *Water Res.* **1982**, *16*, 1099–1105. [CrossRef]
70. Jennings, M.E.; McCutcheon, S.C.; Flynn, K.M. Discussion: Least-Squares Estimates of BOD Parameters. *J. Environ. Eng.* **1982**, *108*, 215–217. [CrossRef]
71. Baulch, D.L.; Bowers, M.; Malcolm, D.G.; Tuckerman, R.T. Evaluated Kinetic Data for High-Temperature Reactions. Volume 5. Part 1. Homogeneous Gas Phase Reactions of the Hydroxyl Radical with Alkanes. *J. Phys. Chem. Ref. Data* **1986**, *15*, 465–592. [CrossRef]
72. Gowda, T.P.H. Modelling Nitrification Effects on the Dissolved Oxygen Regime of the Speed River. *Water Res.* **1983**, *17*, 1917–1927. [CrossRef]
73. O'Connor, D.J.; Dobbins, W.E. Mechanism of Reaeration in Natural Streams. *Trans. Am. Soc. Civ. Eng.* **1958**, *123*, 641–666. [CrossRef]
74. Brenner, A.; Shacham, M.; Cutlip, M.B. Applications of Mathematical Software Packages for Modelling and Simulations in Environmental Engineering Education. *Environ. Model. Softw.* **2005**, *20*, 1307–1313. [CrossRef]
75. Grover, A.S.; Wats, M. Decaying Water Bodies: Victims of Human Neglect or Urbanization. *Int. Proc. Chem. Biol. Environ. Eng.* **2013**, *54*, 48–52.
76. Van Genuchten, M.T.; Leij, F.J.; Skaggs, T.H.; Toride, N.; Bradford, S.A.; Pontedeiro, E.M. Exact Analytical Solutions for Contaminant Transport in Rivers. *J. Hydrol. Hydromech.* **2013**, *61*, 250–259. [CrossRef]
77. Reznickova, J.; Kudrna, V.; Setnickova, K.; Uchytil, P. Evaluation of Diffusivity in Dense Polymeric Membranes by Statistical Moment Analysis. *J. Memb. Sci.* **2013**, *435*, 46–51. [CrossRef]
78. Bhunia, S.; Aghalayam, P. Prediction of Soot for Pressurized Turbulent Kerosene-Air Diffusion Flames Using Method of Moments. *Energy Sources Part A Recovery Util. Environ. Eff.* **2024**, *46*, 3522–3545. [CrossRef]
79. Smith, G.D. *Numerical Solution of Partial Differential Equations: Finite Difference Methods*, 3rd ed.; Oxford University Press: Oxford, UK, 1985.
80. Chapra, S.C. *Surface Water-Quality Modeling*; Waveland Press Inc.: Long Grove, IL, USA, 1997.
81. Von Sperling, M. *Wastewater Characteristics, Treatment and Disposal*; IWA Publishing: London, UK, 2007; Volume 6.
82. Arzhangi, A.; Partani, S.; Danandeh Mehr, A.; Ezzati, F.; Saber, A. Instant Water Quality Index Prediction via Reaeration Process and Hydraulic Parameters in the River System. *Commun. Sustain.* **2026**, *1*, 24. [CrossRef]
83. Wu, J.; Yu, X. Numerical Investigation of Dissolved Oxygen Transportation through a Coupled SWE and Streeter–Phelps Model. *Math. Probl. Eng.* **2021**, *2021*, 6663696. [CrossRef]
84. Thomann, R.V.; Mueller, J.A. *Principles of Surface Water Quality Modeling and Control*; Harper & Row: Manhattan, NY, USA, 1987.
85. Metcalf & Eddy, Inc.; Tchobanoglous, G.; Stensel, H.D.; Tsuchihashi, R.; Franklin, L.B. *Wastewater Engineering: Treatment and Resource Recovery*; McGraw-Hill: Columbus, OH, USA, 2014.
86. Sidorchuk, A.; Panin, A.V. Geomorphological Approach to the River Runoff Evaluation in the Geological Past (Paper 2. Estimation of River Palaeo-Discharges Based on Channel Hydraulics). *Geomorfol. RAS* **2017**, *2*, 3–13. [CrossRef]
87. Dash, S.S.; Khatua, K.K. Sinuosity Dependency on Stage Discharge in Meandering Channels. *J. Irrig. Drain. Eng.* **2016**, *142*, 04016030. [CrossRef]
88. Rantz, S.E. Measurement of Stage and Discharge. In *Measurement and Computation of Streamflow*; United States Department of the Interior: Washington, DC, USA, 1982; Volume 1.
89. Wang, Y.; Huai, W. Estimating the Longitudinal Dispersion Coefficient in Straight Natural Rivers. *J. Hydraul. Eng.* **2016**, *142*, 04016048. [CrossRef]
90. da Silva, G.I.M.; Mannich, M.; Perez, A.B.A.; Chaffe, P.L.B. Longitudinal Dispersion Coefficient Based on Hydraulic Geometry of Streams and Rivers. *Adv. Water Resour.* **2025**, *205*, 105065. [CrossRef]
91. Sahay, R.R. Predicting Longitudinal Dispersion Coefficients in Sinuous Rivers by Genetic Algorithm. *J. Hydrol. Hydromech.* **2013**, *61*, 214–221. [CrossRef]
92. Bahadur, R.; Monteith, M.C.; Samuels, W.B. Comparative Review of Longitudinal Dispersion Coefficient Equations in Rivers. *J. Environ. Eng.* **2021**, *147*, 04021030. [CrossRef]

93. Jiménez Jaramillo, M.A. *MUTC-Un Modelo de Transporte de Rios: Aplicación al Rio Sinú*; Universidad Nacional de Colombia: Medellín, Colombia, 2008.
94. McQuivey, R.S.; Keefer, T.N. Simple Method for Predicting Dispersion in Streams. *J. Environ. Eng. Div.* **1974**, *100*, 997–1011. [CrossRef]
95. Seo, I.W.; Cheong, T.S. Predicting Longitudinal Dispersion Coefficient in Natural Streams. *J. Hydraul. Eng.* **1998**, *124*, 25–32. [CrossRef]
96. Koussis, A.D.; Rodríguez-Mirasol, J. Hydraulic Estimation of Dispersion Coefficient for Streams. *J. Hydraul. Eng.* **1998**, *124*, 317–320. [CrossRef]
97. Kashefipour, S.M.; Falconer, R.A. Longitudinal Dispersion Coefficients in Natural Channels. *Water Res.* **2002**, *36*, 1596–1608. [CrossRef] [PubMed]
98. Gualtieri, C.; Mucherino, C. Comments on "Development of an Empirical Equation for the Transverse Dispersion Coefficient in Natural Streams" by Tae Myoung Jeon, Kyong Oh Baek and Il Won Seo. *Environ. Fluid Mech.* **2007**, *8*, 97–100. [CrossRef]
99. Ushiki, N.; Jinno, M.; Fujitani, H.; Suenaga, T.; Terada, A.; Tsuneda, S. Nitrite Oxidation Kinetics of Two Nitrospira Strains: The Quest for Competition and Ecological Niche Differentiation. *J. Biosci. Bioeng.* **2017**, *123*, 581–589. [CrossRef] [PubMed]
100. Sun, H.; Zhang, H.; Shi, W.; Zhang, P.; Yang, H.; Liu, Y.; Ge, S.; Zhang, W. Temperature Affects the Oxidation Kinetics of Co-Cultured Nitrobacter Winogradskyi and Nitrobacter Hamburgensis in Nitrite-Oxidizing Bioreactor. *J. Environ. Chem. Eng.* **2021**, *9*, 106262. [CrossRef]
101. Ryzhakov, A.V.; Kukkonen, N.A.; Lozovik, P.A. Determination of the Rate of Ammonification and Nitrification in Natural Water by Kinetic Method. *Water Resour.* **2010**, *37*, 70–74. [CrossRef]
102. Merbt, S.N.; Auguet, J.C.; Casamayor, E.O.; Martí, E. Biofilm Recovery in a Wastewater Treatment Plant-Influenced Stream and Spatial Segregation of Ammonia-Oxidizing Microbial Populations. *Limnol. Oceanogr.* **2011**, *56*, 1054–1064. [CrossRef]
103. Melching, C.S.; Flores, H.E. Reaeration Equations Derived from U.S. Geological Survey Database. *J. Environ. Eng.* **1999**, *125*, 407–414. [CrossRef]
104. Isaacs, W.P.; GaudyJr, A.F. Atmospheric Oxygenation in a Simulated Stream. *J. Sanit. Eng. Div.* **1968**, *94*, 319–344. [CrossRef]
105. Cadwallader, T.E.; McDonnell, A.J. A Multivariate Analysis of Reaeration Data. *Water Res.* **1969**, *3*, 731–742. [CrossRef]
106. Padden, T.J.; Gloyna, E.F. *Simulation of Stream Processes in a Model River*; Center for Research in Water Resources: Austin, TX, USA, 1971; Volume 72.

Disclaimer/Publisher's Note: The statements, opinions and data contained in all publications are solely those of the individual author(s) and contributor(s) and not of MDPI and/or the editor(s). MDPI and/or the editor(s) disclaim responsibility for any injury to people or property resulting from any ideas, methods, instructions or products referred to in the content.